Analytic and Monte Carlo approximations to the distribution of the first-passage time of drifted diffusion with stochastic resetting and mixed boundary conditions

Juan Magalang [1,2,*] Riccardo Turin [3,*] Javier Aguilar [4,5,6,†] Laetitia Colombani [7]
Daniel Sanchez-Taltavull [1] and Riccardo Gatto [2]

[1]*Department of Visceral Surgery and Medicine, Inselspital, Bern University Hospital, University of Bern, Murtenstrasse 35, Bern 3008, Switzerland*
[2]*Institute of Mathematical Statistics and Actuarial Science, University of Bern, Alpeneggstrasse 22, Bern 3012, Switzerland*
[3]*Group Risk Management, Swiss Re Management Ltd, Mythenquai 50/60, Zurich 8022, Switzerland*
[4]*Dipartimento di Fisica e Astronomia Galileo Galilei, Università degli Studi di Padova, via Marzolo 8, 35131 Padova, Italy*
[5]*Instituto de Física Interdisciplinar y Sistemas Complejos (IFISC, CSIC-UIB), Campus UIB, 07122 Palma de Mallorca, Spain*
[6]*Department of Electromagnetism and Matter Physics and the Instituto Carlos I de Física Teórica y Computacional, Universidad de Granada, E-18071 Granada, Spain*
[7]*Laboratory of Actuarial and Financial Sciences, ISFA, University Claude Bernard Lyon 1, 50 Avenue Tony Garnier, Lyon 69007, France*

(Received 22 August 2024; revised 27 January 2025; accepted 15 April 2025; published 14 May 2025)

This paper introduces two techniques for computing the distribution of the absorption or first passage time of the drifted Wiener diffusion subject to Poisson resetting times to an upper hard wall barrier and to a lower absorbing barrier. The first method, which we call the Padé-partial fraction approximation, starts with the Padé approximation to the Laplace transform of the first passage time distribution, which is then exactly inverted by means of the partial fraction decomposition. The second method, which we call the multiresolution algorithm, is a Monte Carlo technique that exploits the properties of the Wiener process to generate Brownian bridges at increasing levels of resolution. Our numerical study reveals that the multiresolution algorithm has higher efficiency than standard Monte Carlo, whereas the faster Padé-partial fraction method is accurate in various circumstances and provides an analytical formula. Also, a closed-form exact expression for the expected first passage time is derived.

DOI: 10.1103/PhysRevE.111.054117

I. INTRODUCTION

Drift-diffusion processes represent a cornerstone in the mathematical modeling of systems whose evolution includes stochastic components. The central one is Brownian motion and it finds frequent applications in most scientific fields, such as physics [1–5], biology [6–9], insurance mathematics [10–12], and it builds the basis of mathematical finance. Throughout this paper, we will focus on a drifted and bounded Brownian motion for which the particle returns to its original position at random times following the Poisson process. Such stochastic resetting has gained importance in the past decade [13–24]. Particularly, in the context of biology, stochastic resetting has been used to model hunting behavior in animals, where animals return to specific sites to look for food [25]. At the cellular level, this scheme can model cellular focal adhesions [26]. At the biomolecular level, it has been applied to model backtrack recovery in RNA polymerization [27]. In our previous work, we have shown that stochastic resetting can be used to model the role of changes in therapies to palliate drug resistance development [28]. As models and experimental realizations of processes with stochastic resetting continue to emerge [29,30], there is a growing need for more refined approximation and simulation techniques to comprehensively characterize real-world resetting protocols [16], which we tackle to some extent in this paper.

By means of the Laplace transform and of the underlying stochastic differential equation (SDE) [31,32], we are able to derive analytic and Monte Carlo techniques for computing the distribution of the first passage time (FPT) to the null level of the process [33–40]. With other methods existing in the literature, the mean FPT can be obtained analytically. However, biological and medical applications often require a more detailed statistical depiction. In this paper, we focus on estimating the entire FPT distribution, which enables the derivation of additional quantities such as the standard deviation, median, and upper quantiles.

In this context, this article introduces two computational methods for obtaining the probability distribution of the FPT of the drifted Brownian motion subject to Poisson resetting times and to an upper hard wall barrier. The first of these two techniques makes use of the Laplace transform of the FPT [28]. It is difficult to find a general and accurate method for inverting Laplace transforms. Moreover, most methods are purely numerical. Accurate analytical approximation formulas are, however, useful in various situations, for example, for computing sensitivities of the approximated probabilities. Our method uses the Padé approximation and partial fraction decomposition to approximate the Laplace transform. We call it the Padé-partial fraction (PPF) approximation. Besides

*These authors contributed equally to this work.
†Contact author: javier.aguilarsanchez@unipd.it

high computational speed, it provides a simple closed-form expression for the distribution of the FPT. The second method is a Monte Carlo algorithm that exploits a bridge property of the Wiener process, which allows us to obtain a simulated trajectory at increasing level of detail, recursively [41,42]. We call it the multiresolution algorithm (MRA), following the terminology of wavelet analysis. The MRA allows for very high accuracy. We introduce two versions of the MRA: the standard MRA (SMRA), which directly exploits the bridge property of the Wiener process to our model, and the hybrid MRA (HMRA), which starts with the classical Euler-Maruyama algorithm to generate the initial approximation of the FPT and which improves it further by using the MRA.

This paper has the following structure. We first derive the Laplace transform of the FPT (Sec. II). Then we introduce the PPF approximation (Sec. III). This section also presents a simple expression of the mean FPT. Next, we present the SMRA and HMRA (Sec. IV). These methodological sections are followed by an intensive numerical study, aiming to show the accuracy of our techniques (Sec. V). The paper concludes with a summary of results and a discussion on future research (Sec. VI).

Notation

(1) $f^{(k)}(x) = (d/dx)^k f(x)$, for $k = 0, 1, \ldots$, where $f : \mathbb{R} \to \mathbb{R}$.

(2) $\partial_t f(x,t) = (\partial/\partial t) f(x,t)$, $\partial_x^k f(x,t) = (\partial/\partial x)^k f(x,t)$, for $k = 1, 2$, where $f : \mathbb{R} \times [0,\infty) \to \mathbb{R}$.

(3) $\tilde{f}(s) = \int_0^\infty e^{-st} f(t)\, dt$ is the Laplace transform of $f : [0,\infty) \to \mathbb{R}$.

(4) $\delta(x)$ is the Dirac delta function, which assigns mass 1 at $x = 0$ and is null $\forall x \neq 0$.

(5) $X \sim Y$ means that the random variables X and Y have the same distribution.

(6) $f(x) = o(g(x))$, as $x \to a$, means that $\lim_{x\to a} f(x)/g(x) = 0$, where $f, g : \mathbb{R} \to \mathbb{R}$.[1]

II. LAPLACE TRANSFORM OF PROPAGATOR AND MEAN FPT

The distribution of FPTs is often the essential element in the study of absorption phenomena. This distribution crucially depends on the drift-diffusion processes, the number of dimensions of the diffusion space, and the boundary conditions [33,43–45]. Of particular interest are problems with absorbing or reflecting boundaries. Absorbing boundaries are regions in the diffusion space where diffusing particles can enter but cannot leave [46]. Reflecting boundaries are regions in which diffusing particles cannot permeate [47]. In the following, we will focus on problems with mixed boundary conditions, meaning that the process is bounded between one lower absorbing and one upper reflecting boundary.

Obtaining the closed-form expression for the distribution of the FPT is in general difficult, because it involves solving a Fokker-Planck equation with absorbing boundaries [33,44,45]. Nonetheless, we are still able to characterize the FPT through the Laplace transform. In this section, we derive the Laplace transform of the FPT distribution and obtain a formula for its expectation. Starting with the process without resetting, we obtain the Laplace transform of the propagator by solving the Laplace transform of the Fokker-Planck equation with boundary conditions [46] (Sec. II A). From the propagator, we obtain the Laplace transform of the FPT distribution [28,33] that will relate to the process with resetting through the survival probability (Sec. II B). This strategy of obtaining a survival probability with resetting using the nonresetting case has been previously used in literature in different systems such as in an unbounded one-dimensional system [16,18], an interval with absorbing boundaries at both ends [17], and an interval with mixed boundaries [28]. Finally, by using the aforementioned expressions, we show that the expected FPT with resetting can be expressed in terms of the Laplace transform of the FPT distribution without resetting.

A. Laplace transform of the propagator

The underlying stochastic process is the basic Brownian motion or Wiener process with drift, here denoted $Y = \{Y_t\}_{t\geqslant 0}$, which solves the SDE

$$dY_t = v\, dt + \sqrt{2D}\, dW_t, \ \forall t \geqslant 0, \tag{1}$$

with fixed initial condition $Y_0 = x_0 \in (0, 1]$, where the drift v and the volatility D are, respectively, real and nonnegative real constants. We then impose that the paths of this process are bounded between 0 and 1 and use the same name Y for the bounded process. Level 1 is a reflecting boundary of the hard wall type [33]. On the one hand, the definition of this reflecting boundary at the level of the Fokker-Planck equation requires the concept of probability current and will be given in Eq. (4). On the other, the action of the reflecting boundary at the level of a sample path will be provided along with its discretization scheme in Sec. IV C. We refer to Ref. [48] for a detailed discussion of SDEs with reflecting boundaries. We note that this process is neither the formal reflection of a trajectory, as would be the absolute value of a diffusion, nor the regulated Brownian motion. These two cases are described in the introduction of Ref. [49]. Regarding the null level $Y = 0$, it is an absorbing state and our goal is precisely to evaluate the probability of reaching this state.

Our prior work [28] showcases the practical relevance of the model in describing biological phenomena. Specifically, we utilized a drift-diffusion process with mixed boundary conditions to model drug resistance development resulting from mutation—a stochastic process biased toward the survival of the infecting pathogen [50,51]. Our approach employed a bounded drift-diffusion process to quantify changes in therapy efficacy against the mutating infecting pathogen. The reflecting boundary represented perfect therapy, while the absorbing boundary denoted drug failure, since infecting pathogens develop complete resistance to therapies due to mutation [52].

Denote by $p(\cdot, t)$ the probability density of Y_t, $\forall t > 0$, and $p(\cdot, 0) = \delta(\cdot - x_0)$, called the *propagator*. Let $x \in \mathbb{R}$ and $t \geqslant 0$. The forward Kolmogorov or Fokker-Planck equation determines the probability distribution of the process Y and is given by the PDE:

$$\partial_t p(x,t) + v\partial_x p(x,t) - D\partial_x^2 p(x,t) = 0. \tag{2}$$

We refer, e.g., to Ref. [46] for the construction of Eq. (2).

[1]It is implicitly assumed that g is nonnull over some neighborhood of a, if $|a| < \infty$, or for all extreme Large (small) values, if $a = \infty$ $(-\infty)$.

The propagator is indeed a defective probability density, viz. with total mass below 1, because it does not account for the probability mass at the absorption state. This reflects the physical interpretation of Y as the location of a particle moving between two boundaries that,as soon as it touches the absorbing boundary, it gets immediately removed from the system.

Let us further introduce the probability current:

$$J(x,t) = vp(x,t) - D\partial_x p(x,t). \tag{3}$$

This quantity refers to the rate of influx of Brownian particles at position x. The two boundary conditions, absorption at 0 and a hard wall at 1, can be weakly defined in terms of the propagator and the probability current in the following way:

$$p(0,t) = 0 \quad \text{and} \quad J(1,t) = 0, \tag{4}$$

respectively; see, e.g., Chap. 4 of Ref. [31] or [33]. Furthermore, it is known that solving the probability current at the absorbing boundary $x = 0$, $J(0,t)$ will give the FPT distribution [33]. This is related to the derivation of the inverse Gaussian distribution using the method of images [53,54].

Thus we study the solution of the following system of equations:

$$\begin{aligned} \partial_t p(x,t) + v\partial_x p(x,t) - D\partial_x^2 p(x,t) &= 0 \\ p(0,t) &= 0 \\ J(1,t) &= 0 \\ p(x,0) &= \delta(x - x_0), \end{aligned} \tag{5}$$

in which the last equation provides the initial condition. No closed-form solution to Eq. (5) is available. Lemma II.1 provides a closed-form expression for the Laplace transform of the propagator, viz. for $\tilde{p}(x,s) = \int_0^\infty e^{-st} p(x,t)\,dt$, $\forall s \geqslant 0$.

Lemma II.1 (Laplace transform of propagator). Let $x_0 \in (0,1]$, $v \in \mathbb{R}$, $D > 0$, and consider a p solution to Eq. (5). Let $s > -v^2/(4D)$ and define

$$\rho = \frac{v}{2D}, \quad \omega(s) = \sqrt{v^2 + 4Ds}, \quad \theta(s) = \frac{\omega(s)}{2D} = \frac{\sqrt{v^2 + 4Ds}}{2D} \tag{6}$$

and

$$\alpha_\pm(s) = \frac{v \pm \sqrt{v^2 + 4Ds}}{2D} = \frac{v \pm \omega(s)}{2D} = \rho \pm \theta(s). \tag{7}$$

Then the Laplace transform of the propagator is given by

$$\tilde{p}(x,s) = \tilde{p}(x_0,s) \times \begin{cases} \frac{e^{\alpha_+(s)x} - e^{\alpha_-(s)x}}{e^{\alpha_+(s)x_0} - e^{\alpha_-(s)x_0}}, & \forall x \in [0, x_0) \\ \frac{\alpha_+(s)\, e^{\alpha_+(s)(x-1)} - \alpha_-(s)\, e^{\alpha_-(s)(x-1)}}{\alpha_+(s)\, e^{\alpha_+(s)(x_0-1)} - \alpha_-(s)\, e^{\alpha_-(s)(x_0-1)}}, & \forall x \in (x_0, 1], \end{cases} \tag{8}$$

with $\tilde{p}(x_0,s)$ given by

$$\tilde{p}(x_0,s) = \frac{2\sinh(\theta x_0)\{\omega\cosh[\theta(x_0-1)] + v\sinh[\theta(x_0-1)]\}}{\omega^2\cosh(\theta) - v\,\omega\sinh(\theta)}. \tag{9}$$

The ratio ρ is the Péclet number. A proof of Lemma II.1 may be found in Appendix A 1.

B. Stochastic resetting and stopping condition

We now modify the dynamics of the stochastic process $Y = \{Y_t\}_{t\geqslant 0}$ by stochastic resetting. More explicitly, we assume that at random times $T_0 = 0 < T_1 < T_2 < \ldots$, almost surely, the value of the process Y is reset to its initial value x_0. Following Ref. [16], this is expressed through the addition of a new term to the SDE, giving

$$dX_t = (1 - \chi_t)(v\,dt + \sqrt{2D}\,dW_t) + \chi_t(x_0 - X_t), \ \ \forall t \geqslant 0, \tag{10}$$

where

$$\chi_t = \sum_{n=1}^{\infty} \mathbf{1}\{T_n = t\}, \quad \forall t \geqslant 0,$$

where $\mathbf{1}$ denotes the indicator. We assume that the stochastic process $\chi = \{\chi_t\}_{t\geqslant 0}$ is an independent homogeneous Poisson process with rate or intensity $r > 0$. Thus, T_n is the sum of n independent exponential random variables with expectation r^{-1}, for $n = 1, 2\ldots$. Also, X is a regenerative process with Poisson regeneration times. This property is exploited in our Monte Carlo algorithms.

We can now define the FPT of the process with resetting $X = \{X_t\}_{t\geqslant 0}$ by

$$\tau_r = \inf\{t \geqslant 0 \,|\, X_t \leqslant 0\}. \tag{11}$$

It admits a proper probability density denoted f_r, where the subscript $r \geqslant 0$ highlights the dependence on the Poisson rate r. When $r = 0$, we retrieve the dynamic without resetting.

III. LAPLACE TRANSFORM OF FPT DISTRIBUTION AND PPF

Although $\mathsf{E}[\tau_r]$, the mean FPT, properly informs on typical absorption times, this quantity alone does not quantify the uncertainty inherent to the first passage phenomenon. Often, high-order quantiles are more relevant. Thus, beyond the expectation, we aim to acquire the full probability distribution of τ_r. Its Laplace transform is available but there is no obvious and general way of inverting it. The fast Fourier transform (FFT) is a purely numerical method that may not accurately

approximate upper tail quantiles, crucial for many applications. We refer, for example, to Ref. [12] for a numerical comparison of methods for computing a FPT probability for the compound Poisson process perturbed by diffusion.

In this section, we propose and implement a particular approximation to our FPT distribution. We first obtain the Laplace transform of the FPT (Sec. III A), PPF approximation whose inversion will be approximated numerically. The approximated inversion begins with the Padé approximation of the Laplace transform, followed by a partial fraction decomposition of the Padé approximation and then by the simple inversion of the sum of partial fractions (Sec. III B). This is the PPF approximation. One can find some references, in particular, in the engineering literature, on the problem of obtaining approximate Laplace inversions by rational approximations: some early references are [41,55–58].

A. Laplace transform of FPT distribution with resetting

In this section, we first provide the Laplace transform of the FPT distribution, τ_r, and then we give a simplified formula for its expectation.

Proposition III.1 (Laplace transform of FPT distribution with resetting). Assume that X solves the SDE with resetting of Eq. (10), with $X_0 = x_0 \in (0, 1]$, $v \in \mathbb{R}$, $D > 0$, and $r > 0$. Denote by f_r the probability density of the absorption time τ_r defined in Eq. (11). Then its Laplace transform is given by $\forall s > -r$,

$$\begin{aligned}\tilde{f}_r(s) &= \frac{(s+r)\tilde{f}_0(s+r)}{s+r\tilde{f}_0(s+r)} \\ &= \frac{(s+r)\{\omega(s+r)\cosh[\theta(s+r)(x_0-1)] + v\sinh[\theta(s+r)(x_0-1)]\}}{se^{\rho x_0}\{\omega(s+r)\cosh[\theta(s+r)] - v\sinh[\theta(s+r)]\} + r\{\omega(s+r)\cosh[\theta(s+r)(x_0-1)] + v\sinh[\theta(s+r)(x_0-1)]\}},\end{aligned} \tag{12}$$

where $\tilde{f}_0$ is given by $\forall s > -v^2/(4D)$,

$$\tilde{f}_0(s) = e^{-\rho x_0}\frac{\omega(s)\cosh\{\theta(s)(x_0-1)\} + v\sinh\{\theta(s)(x_0-1)\}}{\omega(s)\cosh\{\theta(s)\} - v\sinh\{\theta(s)\}}. \tag{13}$$

A proof of Proposition III.1 may be found in Appendix A 2. We make two short remarks on Proposition III.1. First, because the Laplace transform exists over a neighborhood of the origin, all moments of τ_r exist and determine its distribution unambiguously. In contrast with this, the FPT of the driving drifted Brownian motion, without hard wall reflecting boundary and without resetting, has infinite moments: it is known that although the FPT of the Brownian motion is finite with probability one, its expectation is infinite [33].

We also note the distribution of the model without resetting is obtained continuously, because $\lim_{r\to 0}\tilde{f}_r(s) = \tilde{f}_0(s)$, $\forall s > 0$.

We end this section with the following closed-form expressions for the the first two moments of the FPT with resetting.

Proposition III.2 (First two moments of FPT). Assume that the process X_t solves the SDE with resetting in Eq. (10), with $X_0 = x_0 \in (0, 1]$, $v \in \mathbb{R}$, $D > 0$ and $r > 0$. Then, the first two moments of τ_r in Eq. (11) are given by

$$\mathsf{E}[\tau_r] = \frac{1}{r}\left(\frac{1}{\tilde{f}_0(r)} - 1\right) \text{ and } \mathsf{E}\left[\tau_r^2\right] = \frac{2}{r\tilde{f}_0(r)}\left(\frac{\tilde{f}_0'(r)}{\tilde{f}_0(r)} + \mathsf{E}[\tau_r]\right), \tag{14}$$

where $\tilde{f}_0(r)$ is given in Eq. (13), where

$$\begin{aligned}\frac{\tilde{f}_0'(r)}{\tilde{f}_0(r)} &= \frac{v(x_0-1) + 2D + \omega(r)\tanh\{\theta(r)(x_0-1)\}}{\omega(r)[\omega(r) + v\tanh\{\theta(r)(x_0-1)\}]} \\ &\quad - \frac{2D - v + \omega(r)\tanh\{\theta(r)\}}{\omega(r)[\omega(r) - v\tanh\{\theta(r)\}]}\end{aligned} \tag{15}$$

and where ρ, ω, and θ are given in Eq. (6).

A proof of Proposition III.2 and the alternative formulas' to Eq. (14) for the moments can be found in Appendix A 3. Thus, we obtain the standard deviation $\sigma_r = \sqrt{\mathsf{E}[\tau_r^2] - \mathsf{E}^2[\tau_r]}$. While σ_r is not used in this paper, it holds clear practical interest. Variability intervals $[\mu_r - 2\sigma_r, \mu_r + 2\sigma_r]$ offer more information than μ_r, often the only given indicator.

B. PPF approximation to FPT distribution with resetting

Because we cannot invert the Laplace transform $\tilde{f}_r$ in Eq. (12) analytically, we now propose to approximate $\tilde{f}_r$ by a specific rational function, which is the ratio of two polynomials with the degree in the denominator higher than in the numerator. The type of rational approximation considered here is the one suggested by Henri Padé's thesis in 1892—the Padé approximation. It has shown practical relevance in many problems of theoretical physics where power series expansions occur, as already stressed by Ref. [59]. Introductions can be found in various books, such as in Sec. 4.6 of Ref. [60], in which it is mentioned that for a given computational time, the Padé approximation is typically more accurate than the Taylor approximation. It has a local error of order smaller than the sum of the two degrees of the two polynomials of the ratio. We note that available tables do not provide the analytical form of the Laplace inverse of a Taylor approximation and,

under some assumptions, they provide the Laplace inverse of many rational functions.

Let m, n be nonnegative integers, let I be an interval of $\mathbb{R}$ with $0 \in I$, and let $g : I \to \mathbb{R}$ be an $n+m$ times differentiable function. Then the Padé approximation of orders m and n to g is the rational function

$$g_{m,n}(s) = \frac{p_m(s)}{q_n(s)}, \tag{16}$$

where

$$p_m(s) = \sum_{j=0}^{m} a_j s^j \text{ and } q_n(s) = \sum_{j=0}^{n} b_j s^j, \quad \forall s \in I,$$

and which satisfies $g^{(k)}(0) = g^{(k)}_{m,n}(0)$ for $k = 0, \ldots, n+m$.[2] It can be shown that these conditions imply that the coefficients $a_0, \ldots, a_m$ and $b_0, \ldots, b_{n-1}$ are obtained by solving the $m+n+1$ linear equations:

$$\sum_{j=0\vee(i-n)}^{i} \frac{g^{(j)}(0)}{j!} b_{i-j} = a_i, \text{ for } i = 0, \ldots, m$$

$$\sum_{j=0\vee(i-n)}^{i} \frac{g^{(j)}(0)}{j!} b_{i-j} = 0, \text{ for } i = m+1, \ldots, m+n. \tag{17}$$

It can also be shown that

$$g(s) - g_{m,n}(s) = o(s^{m+n}), \quad \text{as} \quad s \to 0.$$

The PPF considers the restriction $m < n$. It allows for exact inversion of the Laplace transform in Eq. (12) approximated by Padé and reexpressed in terms of partial fractions. This leads to a simple and practical approximate closed-form expression for the density of the FPT τ_r. Precisely, let $g_{m,n} = p_m/q_n$ be the Padé approximation of orders $m < n$ to the Laplace transform $\tilde{f}_r$. If all roots of q_n are negative, then there exists a Laplace inversion of $g_{m,n}$, which we denote $f_{m,n}$. Thus, $f_{m,n}$ provides an approximation to the density of τ_r, namely, to f_r on $[0, \infty)$. Thus, the density $f_{m,n}$ can be obtained by the following steps, under the above condition on roots of q_n.

Algorithm III.3 PPF approximation to FPT density.

Step 1. Padé approximation

(1) Select the orders $m < n$ of the Padé approximation to $\tilde{f}_r$, which we denote $g_{m,n}$.

(2) Compute $\tilde{f}_r^{(k)}(0)$ for $k = 0, \ldots, n+m$.

(3) Find the coefficients $a_0, \ldots, a_m$ and $b_0, \ldots, b_{n-1}$ by solving the $m+n+1$ linear equations in Eqs. (17).

Step 2. Partial fraction decomposition

(1) Decompose the Padé approximation in partial fractions as follows:

$$g_{m,n}(u) = \frac{p_m(u)}{q_n(u)} = \sum_{j=1}^{k} \sum_{i=1}^{l_j} \frac{\gamma_{j,i}}{(u-\alpha_j)^i}, \tag{18}$$

where $\alpha_1, \ldots, \alpha_k$ are the distinct roots of the denominator q_n, whose multiplicities, respectively, are $l_1, \ldots, l_k$ (with $l_1 + \ldots + l_k = n$).

[2]Note that these same equations hold for the Taylor approximation of order $m+n$.

(2) Compute the real coefficients $\gamma_{j,i}$ for $j = 1, \ldots, k$ and $i = 1, \ldots, l_j$. Typically, q_n has n distinct roots $\alpha_1, \ldots, \alpha_n$. In this case,

$$\frac{p_m(u)}{q_n(u)} = \sum_{j=1}^{n} \frac{\gamma_j}{u-\alpha_j},$$

gives us

$$\gamma_j = \frac{p_m(\alpha_j)}{\prod_{k=1,k\neq j}^{n}(\alpha_j - \alpha_k)}, \quad \text{for } j = 1, \ldots, n.$$

Should not all roots of q_n be distinct, then the coefficients $\gamma_{j,i}$, for $i = 1, \ldots, l_j$ and $j = 1, \ldots, k$, could be obtained a more general formula (cf., e.g., Ref. [61], pp. 233–234).

Step 3. Inversion

This step is only possible under the restriction $\alpha_1, \ldots, \alpha_k < 0$.

(1) Invert the Padé approximation $g_{m,n}$ to $\tilde{f}_r$ by exploiting its reexpression in Eq. (18) so as to obtain the linear combination of gamma or exponential densities:

$$f_{m,n}(t) = \sum_{j=1}^{k} \sum_{i=1}^{l_j} \frac{\gamma_{j,i}}{(i-1)!} t^{i-1} e^{\alpha_j t}, \quad \forall t > 0. \tag{19}$$

Step 4. Corrections

The following corrections to Eq. (19) generally improve its accuracy. To keep the notation simple, the same name $f_{m,n}$ is used for the original approximation of Eq. (19) and for the corrected version.

(1) *Truncation of negative parts*

Negative values are equated to null, viz.

$$f_{m,n}(t) = \max\{f_{m,n}(t), 0\}, \ \forall t > 0.$$

(2) *Smoothing near to origin*

Oscillations near to the origin are removed. Find $s > 0$ the abscissa point of the last local minimum of $f_{m,n}$. If it does not exist, then no correction is required. Consider

$$f_{m,n}(t) = \begin{cases} 0, & \text{if } t \leqslant s \\ f_{m,n}(t), & \text{if } t > s. \end{cases} \tag{20}$$

(3) *Normalization*

Consider

$$f_{m,n}(t) = \left(\int_0^\infty f_{m,n}(s) ds \right)^{-1} f_{m,n}(t), \ \forall t > 0.$$

(4) *Recentering to expectation*

Compute $\mu = \mathsf{E}[\tau_r]$ through its closed-form expression in Eq. (14) and compute $\mu_{m,n}$, the mean of the approximate density $f_{m,n}$. Obtain the recentered approximated FPT density by

$$f_{m,n}(t) = f_{m,n}(t + \mu_{m,n} - \mu), \ \forall t > \max\{0, \mu - \mu_{m,n}\}.$$

Let us now provide some further and more precise justifications to the PPF Algorithm III.3. The PPF approximation $f_{m,n}$ to the FPT density f_r is implicitly defined through its Laplace inversion formula $g_{m,n}(u) = \int_0^\infty e^{-ut} f_{m,n}(t)\, dt$,

$\forall u \geqslant 0$. If $\alpha_1, \ldots, \alpha_k < 0$, then we have

$$\int_0^\infty \frac{t^{i-1}}{(i-1)!} e^{(\alpha_j - u)t}\, dt = \frac{1}{(u-\alpha_j)^i}, \ \forall u > \max\{\alpha_1, \ldots, \alpha_k\}$$

for $i = 1, \ldots, l_j$ and $j = 1, \ldots, k$, This and the partial fractions decomposition of $g_{m,n}$ in Eq. (18) give Eq. (19) in Step 3.

Next, the two corrections regarding truncation to nonnegative values and smoothing near the origin concern only small neighborhoods of the origin. The corrections are due to the fact that the PPF approximation can display undesirable oscillations over these neighborhoods. However, we know that the true FPT density must vanish at the origin. Indeed, the process starts above zero. In addition, repeated Monte Carlo experiments have confirmed that the FPT density is smooth close to the origin and overall unimodal. Based on this theoretical or empirical evidence, the above smoothing correction assumes that the domain of the density is cut in two parts: the region where it increases from null to the maximum of the density, followed by the region where it decreases to null. Accordingly, we correct near the origin by finding the set of points $t > 0$ such that $f'_{m,n}(t) = 0$. We assume that the largest value in this set is a mode of the approximate density and so all other values of the set must be local extrema. If this set has one element only, then no correction is needed. Otherwise, we denote $t^\ddagger$ to be the second-largest value in this set (which is either the last local minimum before the mode or the last point of inflection): We remove the nonmonotonic part around the origin through Eq. (20).

We conclude with the next remarks.

Remarks III.4.

(1) As mentioned, $f_{m,n}$ is not necessarily a probability density: as $\gamma_1, \ldots, \gamma_n$ can be negative, $f_{m,n}$ can be negative over some regions. However,

$$\int_0^\infty f_{m,n}(t)dt = \sum_{j=1}^{k} \sum_{i=1}^{l_j} \frac{\gamma_{j,i}}{(-\alpha_j)^i} = g_{m,n}(0) \longrightarrow \tilde{f}_r(0) = 1, \ \text{as } m, n \to \infty,$$

so the sequence of PPF approximations has the correct normalization in the limit of large m, n.

(2) If the PPF approximation $f_{m,n}$ is a proper probability density, then its expectation is $\mu_{r,m,n}$, given in Eq. (21) below.

(3) If the function $f_{m,n}$ has a Laplace transform of the form of the Padé approximation Eq. (16), i.e., if $f_{m,n} = p_m/q_n$ for some polynomials p_m and q_n, then $f_{m,n}$ is characterized as the solution of the homogeneous linear ordinary differential equation (ODE)

$$f^{(k)}_{m,n}(t) + c_{k-1} f^{(k-1)}_{m,n}(t) + \ldots + c_1 f'_{m,n}(t) + c_0 = 0,$$

for some coefficients $c_0, \ldots, c_{k-1} \in \mathbb{R}$ with $c_0 \neq 0$ and for some positive integer k. Thus, the closeness of $g_{m,n}$, obtained in Step 3, to f_r, the true density, can be reexpressed in terms of closeness of the solution of the above ODE to the true density. This may give another way of analyzing the error of the PPF approximation.

(4) For the process without hard wall and resetting (Y), the FPT follows an inverse Gaussian distribution. In this case, the PPF becomes meaningless. If we consider the process without either hard wall or resetting (Y), but not without the two together, then it remains interesting to compute the FPT distribution and the PPF can be adapted accordingly. These remarks extends to the Monte Carlo MRA of Sec. IV.

(5) The first and second moments of the PPF before correction Eq. (19) are given by

$$\mu_{r,m,n} = \mu^{(1)}_{r,m,n} = \sum_{j=0}^{k} \sum_{i=1}^{l_j} i \frac{\gamma_{j,i}}{(-\alpha_j)^{i+1}}, \tag{21}$$

$$\mu^{(2)}_{r,m,n} = \sum_{j=0}^{k} \sum_{i=1}^{l_j} i(i+1) \frac{\gamma_{j,i}}{(-\alpha_j)^{i+2}}. \tag{22}$$

Details on their derivations are in Appendix A 4.

IV. MRAs

We will see that although the PPF approximation is efficient and provides analytical formulas, it is only valid for specific combinations of the models parameters. Monte Carlo methods are, in general, a good alternative to compute the distribution of any FPT, however, they are computationally intensive. In this section, we propose a Monte Carlo method, MRA, which leads to arbitrary accuracy and a combination of the MRA and the Euler-Maruyama algorithm, which reduces its computational time while keeping the accuracy.

A. MRA for the Wiener process

We describe a particular strategy for generating trajectories of Wiener processes, yielding the SMRA. We provide an algorithm that allows the generation of a single sample path of the Wiener process with arbitrary resolution. The algorithm is directly obtained from the following well-known property of the Wiener process:

$$\mathrm{P}[W_{t+h} \in (x, x+dx) | W_t = a, W_{t+2h} = b] = \frac{1}{\sqrt{\pi h}} \exp\left\{ -\frac{\left(x - \frac{a+b}{2}\right)^2}{h} \right\} dx, \ \forall t, h > 0, a, b \in \mathbb{R}. \tag{23}$$

Therefore, given the states of the process at two times ($W_t = a$ and $W_{t+2h} = b$), Eq. (23) allows us to sample the process at intermediate middle time (W_{t+h}). This property can be iterated to access arbitrary small temporal scales, as sketched in Fig. 1, and we will use it to obtain approximations to the FPT at arbitrary accuracy. Indeed, consider the stopping time

$$T = \inf\{t \geqslant 0 \mid W_t \leqslant 0\},$$

where we slightly alter the standard definition of the Wiener process to have some initial point $x_0 > 0$ that makes T nontrivial. Let us assume that a discretization $\{W_{nh}\}_{n=1,2,\ldots}$ of $\{W_t\}_{t \geqslant 0}$ is available for some $h > 0$ small. Then,

$$T_h = \inf\{t \geqslant 0 \mid W_{nh} \leqslant 0\}$$

is an overestimation of T (precisely $T_h \geqslant T$ a.s.) that converges to T, as $h \to 0$. This tells us that applying the MRA at increasing resolutions allows us to approximate the stopping time at any desired precision.

k	2^k+1	$W_{k,j}$
0	2	$W_{0,0}$ $W_{0,1}$
1	3	$W_{1,0}$ $W_{1,1}$ $W_{1,2}$
2	5	$W_{2,0}$ $W_{2,1}$ $W_{2,2}$ $W_{2,3}$ $W_{2,4}$
3	9	$W_{3,0}$ $W_{3,1}$ $W_{3,2}$ $W_{3,3}$ $W_{3,4}$ $W_{3,5}$ $W_{3,6}$ $W_{3,7}$ $W_{3,8}$

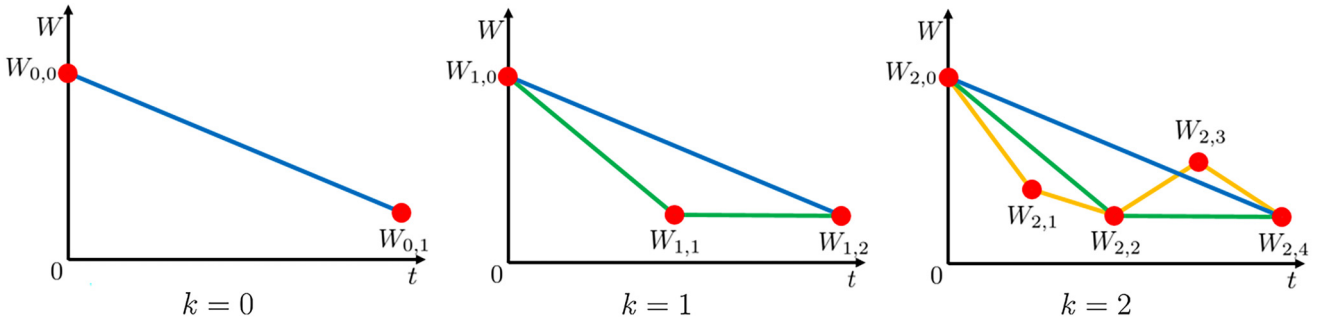

FIG. 1. Upper table: Resolution level k and corresponding number of generated variables 2^k+1 (first two columns); generated variables $W_{k,j}$ (last column). Equal signs indicate copying a variable from a previous resolution; see Eq. (25a). Arrows indicate generating a new variable from a previous resolution; see Eq. (25b). Lower graphs: Illustrations of the trajectory generated subsequently by the MRA.

For a given time interval, for example, $t \in [0, 1]$, we denote k the resolution level of the sample path on that interval as $\mathbf{W}_k = \{W_{k,j}\}$ for $j = 0, 1, \ldots, 2^k$ and $k = 0, 1, \ldots$. The two indices allow us to evaluate the process at the particular time $t = 2^{-k} j \in [0, 1]$, through $W_{k,j} = W_{t=2^{-k}j}$. The first index k provides the level of refinement or resolution of the path. The second index j refers to the ordinal within the resolution level k. Therefore, at initial level $k = 0$, we have

$$\mathbf{W}_0 = \{W_{0,0}, W_{0,1}\}, \tag{24}$$

where $W_{0,0} = 0$ and $W_{0,1} \sim \mathcal{N}(0, 1)$. Here, $\mathcal{N}(\mu, \sigma^2)$ stands for a Gaussian random variable with mean μ and variance σ^2. Then, consecutive levels of refinement, $k \geqslant 1$, are obtained by

$$W_{k,2j} = W_{k-1,j}, \qquad \text{for } j = 0, 1, \ldots, 2^{k-1} \tag{25a}$$

$$W_{k,2j+1} \mid W_{k-1,j}, W_{k-1,j+1} \sim \mathcal{N}\left(\frac{W_{k-1,j} + W_{k-1,j+1}}{2}, \frac{1}{2^k}\right), \quad \text{for } j = 0, 1, \ldots, 2^{k-1} - 1. \tag{25b}$$

The precise meaning of Eq. (25b) is that the *conditional* distribution of $W_{k,2j+1}$, *given* $W_{k-1,j}$ and $W_{k-1,j+1}$, is Gaussian with mean $(W_{k-1,j} + W_{k-1,j+1})/2$ and variance $1/2^k$. For $k > 0$, the even indices of j are copied over as the resolution increases, as in Eq. (25a). The odd indices of j are generated randomly using two consecutive variables from the previous resolution, as in Eq. (25b). Proceeding in this way, the overestimation of the FPT of $\mathbf{W}_k$ decreases as k increases.

Further details about the MRA can be found in pp. 277–279 of Ref. [42]. In Appendix B 1, we show a pseudocode with the implementation of the MRA for the process $\{W_t\}_{t\geqslant 0}$.

B. MRA with resetting

This section describes the application of the MRA to a process with resetting, similar to the one of Sec. II A, but without considering the reflecting boundary for now. Let us call $\{B_t\}_{t\geqslant 0}$ the drifted Brownian motion without hard wall and without resetting,

$$dB_t = v\, dt + \sqrt{2D}\, dW_t, \ \forall t \geqslant 0, \tag{26}$$

where $B_0 = x_0 > 0$. Let us call $\mathbf{t}^\dagger$ the sequence of times at which the process experiences a reset,

$$\mathbf{t}^\dagger = \{t_0^\dagger, t_1^\dagger, t_2^\dagger, \ldots\},$$

where $t_0^\dagger = 0$, $(t_{i+1}^\dagger - t_i^\dagger) \sim \text{Exponential}(1/r)$. Let us define reset intervals from pairs of consecutive reset times: $\{(0, t_1^\dagger), (t_1^\dagger, t_2^\dagger), \ldots\}$. The main idea to exploit is that B_t is a normally distributed random variable with mean $\mu = x_0 + vt$ and variance $\sigma^2 = 2Dt$ within any reset interval. Therefore, we can build Brownian bridges connecting the extremes of reset intervals with arbitrary precision. We first consider the process in the first reset interval, $t \in [0, t_1^\dagger]$, and, similar to the Wiener process in Sec. IV A, we define the kth resolution level

of the sample path in that interval as $\mathbf{B}_k^{(1)}$. In the first resolution level, the process starts at the initial position, $B_{0,0} = x_0$, with initial time 0, and ends at the final position, $B_{0,1}$, with final time $t_1^\dagger$. Therefore,

$$\mathbf{B}_0^{(1)} = \{B_{0,0}^{(1)}, B_{0,1}^{(1)}\}, \tag{27}$$

where $B_{0,1}^{(1)} \sim \mathcal{N}(x_0 + vt_1^\dagger, 2Dt_1^\dagger)$. Then, similar to Eq. (25), the generation of the process at the next resolution k is obtained by

$$B_{k,2j}^{(1)} = B_{k-1,j}^{(1)}, \quad \text{for } j = 0, 1, \ldots, 2^{k-1}, \quad \text{and} \tag{28a}$$

$$B_{k,2j+1}^{(1)} \sim \mathcal{N}\left(\frac{B_{k-1,j}^{(1)} + B_{k-1,j+1}^{(1)}}{2}, \frac{2Dt_1^\dagger}{2^k}\right), \quad \text{for } j = 0, 1, \ldots, 2^{k-1} - 1. \tag{28b}$$

The same steps can be used to generate the Brownian trajectory in the second reset interval, $\mathbf{B}_k^{(2)}$, simply replacing $t_1^\dagger$ by $t_2^\dagger - t_1^\dagger$ in Eqs. (27) and (28b). In general, the Brownian trajectory in the ith reset interval, i.e., $(t_i^\dagger, t_{i-1}^\dagger)$, and at refinement level k is obtained through

$$\mathbf{B}_0^{(i)} = \{B_{0,0}^{(i)}, B_{0,1}^{(i)}\}, \tag{29}$$

where $B_{0,1}^{(i)} \sim \mathcal{N}(x_0 + v(t_i^\dagger - t_{i-1}^\dagger), 2D(t_i^\dagger - t_{i-1}^\dagger))$, and

$$B_{k,2j}^{(i)} = B_{k-1,j}^{(i)}, \quad \text{for } j = 0, 1, \ldots, 2^{k-1}, \quad \text{and} \tag{30a}$$

$$B_{k,2j+1}^{(i)} \sim \mathcal{N}\left(\frac{B_{k-1,j}^{(i)} + B_{k-1,j+1}^{(i)}}{2}, \frac{2D(t_i^\dagger - t_{i-1}^\dagger)}{2^k}\right), \quad \text{for } j = 0, 1, \ldots, 2^{k-1} - 1. \tag{30b}$$

Since $B_{k,2^k}^{(i-1)} \neq B_{k,0}^{(i)} = x_0$, the procedure described so far generates a multivalued process when consecutive reset intervals are concatenated. Therefore, once the multiresolution algorithm has been applied until the desired level of resolution, we obtain the proper discretization of the process setting $B_{k,2^k}^{(i)} = x_0$ for $i = 0, 1, \ldots$.

C. Reflecting boundary

We now add the hard wall reflecting boundary [33] to the previous developments. The hard wall reflections that bound the process below level 1 annihilate the Gaussian nature of the process, which is essential to the multiresolution method. To solve this issue, we first generate an unbounded trajectory with the multiresolution method $\mathbf{B}_k^{(i)}$ at some resolution level $k \geqslant 1$. Then, by using increments of $\mathbf{B}_k^{(i)}$, we define the reflected process $\mathbf{R}_k^{(i)}$ as follows:

$$R_{k,j+1}^{(i)} = \begin{cases} R_{k,j}^{(i)} + \Delta B_{k,j}^{(i)}, & \text{if } R_{k,j}^{(i)} + \Delta B_{k,j}^{(i)} \leqslant 1 \\ 2 - (R_{k,j}^{(i)} + \Delta B_{k,j}^{(i)}), & \text{if } R_{k,j}^{(i)} + \Delta B_{k,j}^{(i)} > 1 \end{cases}$$
$$= \min\left\{R_{k,j}^{(i)} + \Delta B_{k,j}^{(i)}, 2 - \left(R_{k,j}^{(i)} + \Delta B_{k,j}^{(i)}\right)\right\}, \tag{31}$$

where $\Delta B_{k,j}^{(i)} = B_{k,j+1}^{(i)} - B_{k,j}^{(i)}$ for $j = 0, \ldots, 2^{k+1}$, and $R_{k,0}^{(i)} = x_0$.

D. Stopping condition

Every resolution k will provide a value for the first time at which the trajectory $\mathbf{R}_k$ is observed to go below the absorbing boundary, which is the null line:

$$\tau_{r,k} = \inf\left\{t_{k,j}^{(i)} \in (t_{i-1}^\dagger, t_i^\dagger) \,|\, R_{k,j}^{(i)} \leqslant 0,\ i = 1, 2, \ldots\right\}. \tag{32}$$

This time provides an approximation to the target FPT at resolution k. Increasing the resolution yields finer sample paths and therefore finer estimations according to Eq. (32). However, we note that estimations using Eq. (32) are always upper bounds to the real FPT. Furthermore, if $k > k'$, then

$$\tau_r \leqslant \tau_{r,k} \leqslant \tau_{r,k'}.$$

This inequality has important consequences for our simulation schemes. Basically, every estimation induces an effective time horizon for our Monte Carlo method. Given the estimation at some resolution k, $\tau_{r,k}$, it makes no sense to simulate the process on times $t > \tau_{r,k}$ since $\tau_r \leqslant \tau_{r,k}$.

An explicit condition at which we may stop the simulation can be defined by using an error threshold $\epsilon > 0$. We define the maximum resolution level $k^\dagger$ such that the time increment is below ϵ,

$$k^\dagger = -\left\lceil \frac{\ln(\epsilon)}{\ln(2)} \right\rceil,$$

where $\lceil x \rceil$ denotes the smallest integer $\geqslant x$.

We finally define all elements required to use the MRA to sample the FPT—we denote this version of the algorithm as the SMRA. We start by generating the unbounded motion from Eq. (26) in the first reset interval ($i = 1$) for a target resolution $k^\dagger$ using Eq. (30). Once the Brownian trajectory has been generated in the first reset interval, we compute the reflected process in this interval through Eq. (31). If the stopping condition in the first interval is reached, cf. Eq. (32), then the simulation stops and we can sample an estimation for the FPT at resolution $k^\dagger$. Otherwise, we draw the next reset time, $t_2^\dagger$, and proceed similarly in the second reset interval (i.e., generating the Brownian trajectory using the multiresolution scheme, then reflecting the trajectory and, lastly, checking if

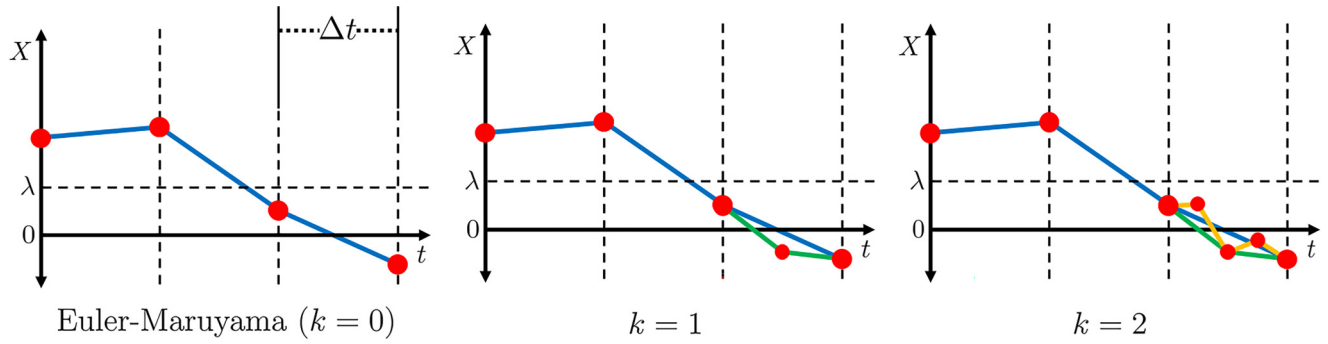

FIG. 2. Illustrations of trajectories generated from HMRA. Time increments of the Euler-Maruyama algorithm (Δt) are sketched as the separation of vertical dashed lines.

the reflecting trajectory reaches the stopping criteria). This procedure is iterated until the stopping condition is reached.

Once the above process is used to get an estimation of the FPT with resolution $k^\dagger$, $\tau_{r,k^\dagger}$, it can be further refined to reach a new resolution level $k > k^\dagger$. In this second phase, there are no further sampling of reset times, and the multiresolution scheme is iterated on a fixed interval $[0, \tau_{r,k^\dagger}]$. This is because $\tau_{r,k^\dagger}$ is an upper bound for the true FPT.

E. HMRA

Stochastic resetting can strongly increase the computational requirements of the SMRA. This is because it requires applying the multiresolution method in multiple reset intervals with a high resolution $k^\dagger$, which is especially costly when $1/r \ll \tau_r$ because it results in a large number of resets.

The Euler-Maruyama algorithm partially overcomes these limitations, however, it tends to overestimate the FPT and does not have an arbitrary accuracy. We propose the HMRA that refines the Euler-Maruyama trajectories with the MRA (Fig. 2). In doing so, first we produce a trajectory of the Euler-Maruyama (Algorithm 3), with a time step Δt. Close to the absorbing boundary (i.e., below some small positive level), we use the MRA to refine the approximation. The details are provided in Appendix B 5.

Note, finally, that with our process the higher order Milstein scheme reduces to the Euler-Maruyama, because the coefficient of dW_t in Eq. (1), $\sqrt{2D}$, does not depend on X_t.

V. NUMERICAL RESULTS

To illustrate the effectiveness of the PPF, the SMRA, and the HMRA, we empirically study their performance in terms of accuracy, memory requirements, and speed. Source codes and PYTHON packages of the PPF and MRA are available in the links provided in Appendixes A and B.

A. PPF

The results of the approximation at order $m = 2$ and $n = 3$ are shown in Figs. 3(a) and 3(b), which are compared with simulated results of the HMRA. In Fig. 3 and Table I, we observe that the PPF method is a good approximation of the entire distribution obtained by Monte Carlo, for multiple values of v, except for the percentile $p = 0.1$, for negative values of v. Furthermore, we observe that the analytical second moments of the PPF in Eq. (21) and Monte Carlo also approximate the analytical second moment in Eq. (14). For the multiple values of v computed in Fig. 3, the maximum relative change of both the PPF and Monte Carlo second moments, with respect to the analytical second moment, are found at $v = -3 \times 10^{-3}$. These measures of relative change are 1.193×10^{-12} and 1.063×10^{-2}, respectively. Further details may be found at the proof for the moments for the PPF in Appendix A.

For a valid result from the PPF method, we need to identify all the roots of the denominator of the Padé approximation and ensure that they are real and negative, cf. Step 3 of Algorithm III B. Having at least one positive root implies that no Laplace inverse of $f_{m,n}$ exists. On the other hand, if there is at least one nonreal root, the result yields a damped sinusoidal, i.e., a signed function. By varying drift v and diffusion D values, we obtain the regions (v, D) where the PPF method fails. These regions are shown in Fig. 4. Moreover, Fig. 8 of Appendix A provides the superposition of the two graphs of Fig. 4, thus showing the regions of valid and invalid parameters (v, D). In Figs. 4 and 8, the orders are $m = 2, n = 3$, with resetting rate $r = (1/3) \times (1/365)$.

B. SMRA and HMRA

When comparing the accuracy of SMRA and HMRA by comparing their simulated mean FPT with the analytical mean FPT, we observe that as error threshold ϵ decreases, both algorithms converge to the analytical solution, while very small step sizes are necessary for Euler-Maruyama to reach the same level of accuracy (Fig. 5). In terms of computational requirements, when we decrease ϵ, we observe a linear increase in $\langle k \rangle$ that would lead to an exponential increase in memory requirements as it is proportional to the number of points generated for each trajectory. Therefore, HMRA outperforms SMRA since it needs lesser points to reach the same accuracy [Fig. 6(a)]. Finally, in terms of speed, the HMRA outperforms the MRA by 2 to 4 orders of magnitude [Fig. 6(b)].

Although HMRA outperforms SMRA, HMRA requires two parameters to be set, ϵ and Δt. For this reason, we study the impact of either parameters in terms of computational time. For all values of Δt, we identify where reducing ϵ does not correspond to a significant increase in computational time. However, as ϵ is further decreased, the computational

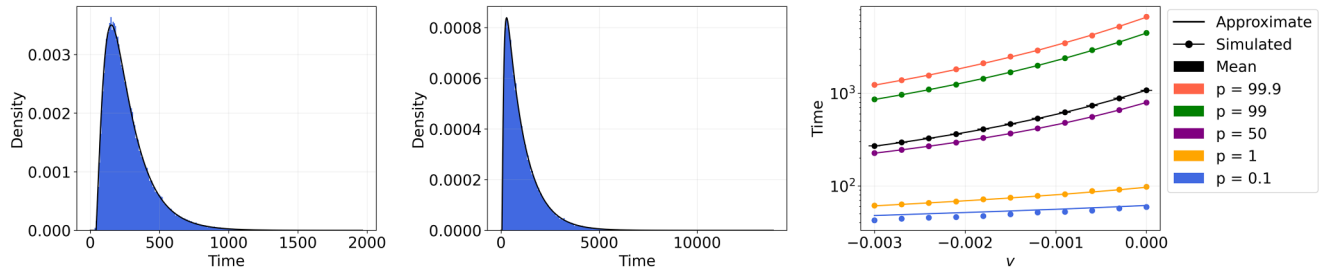

(a) $v = -3 \times 10^{-3}$ (b) $v = 0$ (c)

FIG. 3. Results of PPF approximation; parameters are $D = 5 \times 10^{-4}$, $r = (3 \times 365)^{-1}$ and approximation orders $m = 2$, $n = 3$. (a), (b) Histograms obtained from 10^6 generated values and continuous curves obtained from PPF with varying drift $v = -3 \times 10^{-3}$ and $v = 0$. (c) Comparing quantiles close to the tails, medians, and means generated from PPF and 10^6 simulations for a varying drift.

time rapidly increases by orders of magnitude. This behavior describes a Pareto front, suggesting the existence of a critical value of ϵ which yields the best trade-off between accuracy and speed [Fig. 6(c)].

VI. DISCUSSION

We have addressed the problem of computing the FPT distribution to the null level of the drifted Brownian motion with upper hard wall barrier and Poisson resetting times. In doing so, we first introduced the PPF approximation, which is an analytical formula that can be immediately evaluated. We then introduced the SMRA and HMRA, that are purely numerical but give arbitrary accuracy, and we have shown how they overcome the limitations of some other available methods in terms of accuracy and speed. Moreover, by using the survival function of the FPT, we have found compact expressions for the two first moments of the FPT with resetting. The formulas rely only on the Laplace transform of the FPT without resetting [16,17]. Our derivation is more direct than the one in Ref. [28].

Precisely, with the PPF we have proposed an approximation of the Laplace transform by taking the Padé approximation and its partial fraction decomposition [41]. These steps, followed by exact inversion, yield our PPF approximation. It is accurate and, unlike most methods such as the Talbot approximation [62,63], does not rely on numerical integration, allowing for immediate numerical evaluation. The PPF approximation is limited to a specific parametric region, but we have identified a region where it can be applied. The method generally works for smaller absolute values of v, but increasing this parameter requires greater values of D to remain valid. This region is particularly significant since the processes generated by these parameters are driven by the stochastic effects more than the deterministic drift. An extension that is currently under investigation by some of the authors is an expansion of the region of validity using the fact that complex partial fraction coefficients will always be in conjugate pairs. One may then obtain an inversion even with complex partial fraction coefficients.

To overcome this limitation, we have presented the MRA. Given two consecutive points on a trajectory, a property of Wiener processes is that the intermediate of the two points is Gaussian with mean given by the average of the first and last points [64]. The MRA exploits this bridge property by generating intermediate points between intervals of the trajectory. Hence, the MRA can generate finer values up to any threshold of error compared to other methods for which the level of resolution is fixed in advance [42], making the control of the error difficult.

TABLE I. Upper tail probabilities of HMRA and PPF in Figs. 3(a) (left table) and 3(b) (right table).

t	$P_{HMRA}[\tau_r > t]$	$P_{PPF}[\tau_r > t]$	t	$P_{HMRA}[\tau_r > t]$	$P_{PPF}[\tau_r > t]$
342.140	0.25000	0.24918	1445.966	0.25000	0.25089
379.322	0.19937	0.19800	1664.281	0.19842	0.19894
416.503	0.15806	0.15718	1882.596	0.15738	0.15775
453.685	0.12593	0.12470	2100.911	0.12428	0.12508
490.866	0.10099	0.09891	2319.225	0.09894	0.09919
528.047	0.07981	0.07843	2537.540	0.07823	0.07865
565.229	0.06382	0.06219	2755.855	0.06189	0.06236
602.410	0.05082	0.04931	2974.170	0.04967	0.04945
639.592	0.04064	0.03910	3192.485	0.03972	0.03921
676.773	0.03234	0.03100	3410.800	0.03117	0.03109
713.955	0.02555	0.02458	3629.115	0.02444	0.02465
751.136	0.02020	0.01949	3847.430	0.01964	0.01955
788.317	0.01591	0.01545	4065.745	0.01589	0.01550
825.499	0.01253	0.01225	4284.060	0.01255	0.01229
862.680	0.01000	0.00971	4502.375	0.01000	0.00975

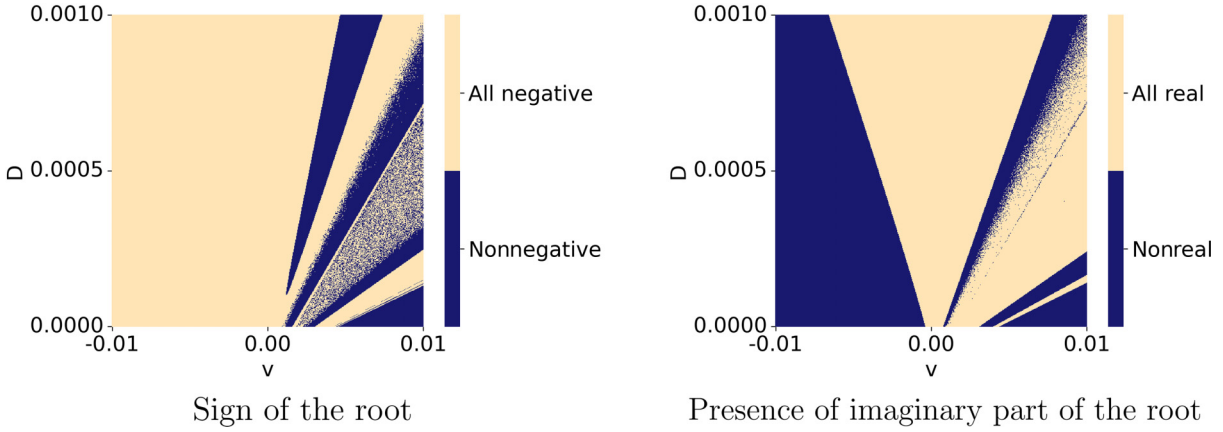

FIG. 4. Regions of the parametric space (v, D) of validity of the PPF with orders $m = 2, n = 3, r = (1/3) \times (1/365)$.

We have introduced two versions of the MRA, namely, the SMRA and HMRA. Both simulation algorithms have shown high accuracy and convergence with respect to the exact analytical mean FPT and the simulation results of the standard Euler-Maruyama algorithm, which is based on a single and very small time increment. It is known that computing the FPT by Euler-Maruyama gives overestimation proportional to the time increment [42]. Thus, both SMRA and HMRA correct this overestimation through the construction of Brownian bridges. Because the SMRA computes the entire sample path over a large time horizon (to obtain the FPT to an arbitrary accuracy), it requires substantial computational resources. To increase speed and memory efficiency, the HMRA proceeds as follows: it first approximates the FPT with Euler-Maruyama and then locally refines the resolution through MRA. This yields a more efficient Monte Carlo technique than either the Euler-Maruyama or SMRA individually. Our Monte Carlo algorithm is particularly well-suited for studying processes that involve both fast and slow absorption pathways, where a fine, uniform time discretization could result in prohibitively expensive simulations. The model we study here demonstrates this combination of fast and slow absorption when the process is biased toward the reflecting boundary and the initial condition is close to the absorbing boundary. A similar combination of fast and slow absorption processes is also observed in Ref. [35].

We note that the PPF method is rather general: it can in principle be applied to other problems where the Laplace transform is available but complicated, so the distribution cannot be obtained. The only restriction comes from the nature of the roots in the partial fraction decomposition. We studied empirically the nature of these roots, depending on values of the model parameters. Such an empirical analysis can, in principle, be done for other models of interest.

Our Monte Carlo methods can readily be used with other Gaussian processes, such as the Ornstein-Uhlenbeck process (see, e.g., pp. 229–230 of Refs. [65,66]). Beyond the FPT, our method could be used to estimate the first passage area, namely, the area enclosed between the null line and the path of the process up to the FPT, that has recently received substantial attention, cf.. e.g., Ref. [67]. We envisage that it would be possible to extend our results to non-Gaussian α-stable Lévy processes using generalizations of the Brownian bridge [68–70]. Lastly, future work could focus on characterizing the optimal parameter choices that balance CPU time consumption and precision, as has been done for jumping processes [71]. As the use of stochastic resetting in empirical studies and complex models increases, so does the need to refine numerical methods for precise calculations within feasible CPU times. We believe the numerical methods proposed here will help advance the characterization of typical scales in processes with stochastic resets, enabling

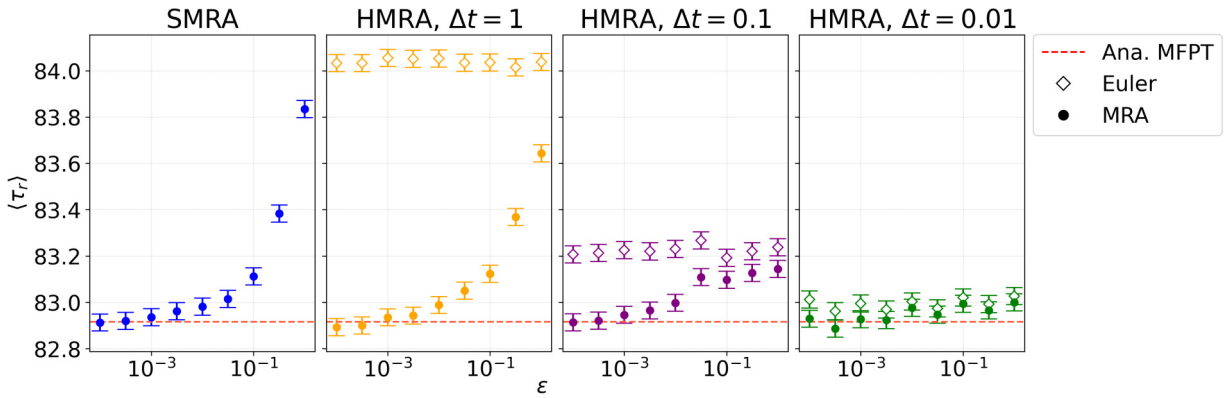

FIG. 5. SMRA and HMRA results in different Euler-Maruyama time steps Δt, with changing threshold ϵ. $v = -10^{-2}$, $D = 10^{-4}$, $r = (3 \times 365)^{-1}$, $x_0 = 0.8$, 10^6 simulations.

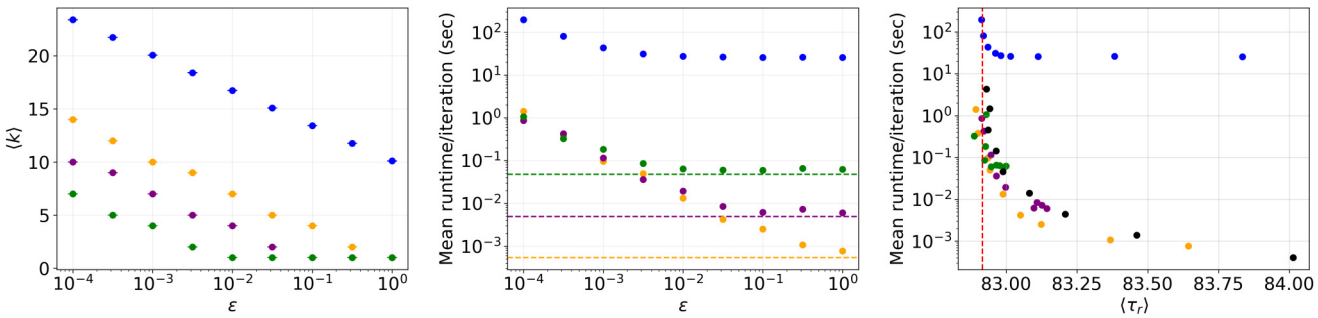

(a) $\langle k \rangle$ (b) Mean runtime per iteration (c) $\langle \tau_r \rangle$ vs mean runtime

FIG. 6. Speed and accuracy comparisons between the SMRA (●), HMRA with $\Delta t = 1$ (●), HMRA with $\Delta t = 0.1$ (●), and HMRA with $\Delta t = 0.01$ (●). (a) Mean resolution per iteration. (b) Mean runtime per iteration. Dashed lines refer to the mean run times of the corresponding first Euler-Maruyama estimates for HMRA. (c) Comparisons between the mean FPT and the mean run time per iteration of different simulation schemes. SMRA and HMRA simulations taken from Fig. 5, Euler-Maruyama (●) plotted simulations with varying Δt, vertical red dashed line is the analytical mean FPT.

calculations with arbitrary precision and efficient computational performance.

ACKNOWLEDGMENTS

The authors thank two reviewers for their important comments and suggestions. They are particularly thankful to D. Ginsbourger for his dedicated support and insightful scientific discussions. This work was supported by the UniBE ID Grant 2021, the Ruth & Arthur Scherbarth Foundation, the Agencia Estatal de Investigación (AEI, MCI, Spain) MCIN/AEI/10.13039/501100011033 and Fondo Europeo de Desarrollo Regional (FEDER, UE) under Project APASOS (No. PID2021-122256NB-C21/C22) and the María de Maeztu Program for units of Excellence in R&D, Grant No. CEX2021–001164-M. MUR - PRIN - NextGenerationEU - Project Title "Emergent Dynamical Patterns of Disordered Systems with Applications to Natural Communities" CUP 2022WPHMXK.

DATA AVAILABILITY

The source code (in PYTHON) for the PPF, SMRA, and HMRA is available on Github through the following links: PPF [72] MRA [73]. Furthermore, the corresponding Python packages can be installed from PyPI at Refs. [74], [75].

APPENDIX A: PROOFS

In this Appendix, we use the following simplified notation: $f'(x,t) = \partial/\partial x f(x,t)$ and $f''(x,t) = (\partial/\partial x)^2 f(x,t)$, where $f : \mathbb{R} \times [0,\infty) \to \mathbb{R}$.

1. Proof of Lemma II.1

Proof. We begin by taking the Laplace transform of Eq. (2) with respect to t and proceed to solve for the propagator using a procedure similar to the method of undetermined coefficients. Denote by $\mathcal{L}$ the operator of Laplace transform. First, note that swapping integral and derivative operation over different variables yields

$$\mathcal{L}(vp'(x,\cdot))(s) = v\tilde{p}'(x,s),$$
$$\mathcal{L}(Dp''(x,\cdot))(s) = D\tilde{p}''(x,s).$$

The first term is the only term in the equation that has a derivative dependent on t, which yields

$$\partial_t p(x,t) = s\tilde{p}(x,s) - p(x,0) = s\tilde{p}(x,s) - \delta(x - x_0),$$

where $p(x,0) = \delta(x - x_0)$, taken from the initial condition in Eqs. (5). Therefore, the transform of Eq. (2) for $\tilde{p}(x,s)$ is given by a nonhomogeneous differential equation

$$s\tilde{p}(x,s) - \delta(x - x_0) + v\tilde{p}'(x,s) - D\tilde{p}''(x,s) = 0, \quad s \geqslant 0 \tag{A1}$$

for $x \in [0, x_0) \cup (x_0, 1]$. Rearranging the equation to have the nonhomogeneous term on the right-hand side, we obtain

$$D\tilde{p}''(x) - v\tilde{p}'(x) - s\tilde{p}(x) = -\delta(x - x_0). \tag{A2}$$

To find a solution to Eq. (A1), let us fix s, denote $\tilde{p}_<(x) = \tilde{p}(x,s)$ for $x \in [0, x_0)$, $\tilde{p}_>(x) = \tilde{p}(x,s)$ for $x \in (x_0, 1]$ and search an analytic solution to the associated homogeneous differential equation to Eq. (A2),

$$D\tilde{p}''(x) - v\tilde{p}'(x) - s\tilde{p}(x) = 0,$$

over these two intervals. The characteristic equation is $D\alpha^2 - v\alpha - s = 0$, with roots, defined in Eq. (7),

$$\alpha_\pm = \frac{v \pm \sqrt{v^2 + 4Ds}}{2D} = \frac{v \pm \omega(s)}{2D} = \rho \pm \theta(s),$$

where the constants are defined by Eq. (6). Therefore,

$$\tilde{p}_>(x) = Ae^{\alpha_+ x} + Be^{\alpha_- x} \quad \text{and} \quad \tilde{p}_<(x) = ae^{\alpha_+ x} + be^{\alpha_- x}$$

for some constants a, b, A, and B to be determined. From the boundary conditions Eq. (4), we obtain

$$\tilde{p}_<(x) = a(e^{\alpha_+ x} - e^{\alpha_- x})$$

and

$$v(Ae^{\alpha_+} + Be^{\alpha_-}) = D(\alpha_+ Ae^{\alpha_+} + \alpha_- Be^{\alpha_-}).$$

The latter equation may be rewritten as

$$(D\alpha_+ - v)Ae^{\alpha_+} = (v - D\alpha_-)Be^{\alpha_-} = C(s),$$

implying

$$\tilde{p}_>(x) = C\left(\frac{e^{\alpha_+(x-1)}}{D\alpha_+ - v} + \frac{e^{\alpha_-(x-1)}}{v - D\alpha_-}\right).$$

The continuity of $p(\cdot, t)$ (see Ref. [32], Chap. 15, Sec. 5) yields $\tilde{p}_<(x_0) = \tilde{p}_>(x_0)$, hence one can write

$$C\left(\frac{e^{\alpha_+(x_0-1)}}{D\alpha_+ - v} + \frac{e^{\alpha_-(x_0-1)}}{v - D\alpha_-}\right) = a(e^{\alpha_+ x_0} - e^{\alpha_- x_0}) = c(s).$$

Consequently, we obtain

$$\tilde{p}_<(x) = c(s)\frac{e^{\alpha_+ x} - e^{\alpha_- x}}{e^{\alpha_+ x_0} - e^{\alpha_- x_0}},$$

$$\tilde{p}_>(x) = c(s)\frac{\frac{e^{\alpha_+(x-1)}}{D\alpha_+ - v} + \frac{e^{\alpha_-(x-1)}}{v - D\alpha_-}}{\frac{e^{\alpha_+(x_0-1)}}{D\alpha_+ - v} + \frac{e^{\alpha_-(x_0-1)}}{v - D\alpha_-}}.$$

Noticing

$$v - D\alpha_- = D\alpha_+ \quad \text{and} \quad v - D\alpha_+ = D\alpha_-,$$

we have

$$\tilde{p}_>(x) = c(s)\frac{\alpha_+ e^{\alpha_+(x-1)} - \alpha_- e^{\alpha_-(x-1)}}{\alpha_+ e^{\alpha_+(x_0-1)} - \alpha_- e^{\alpha_-(x_0-1)}}.$$

Our goal is now to determine the function $c(s) = \tilde{p}(x_0, s)$.

We proceed to examine conditions involving the derivative of p following standard procedures (see, e.g., p. 16 of Ref. [33] or p. 449 of Ref. [76]). We now return to the nonhomogeneous differential equation in Eq. (A2). Integrating the above equation on a segment around x_0,

$$\int_{x_0-\epsilon}^{x_0+\epsilon} \{D\tilde{p}''(x, s) - v\tilde{p}'(x, s) - s\tilde{p}(x, s)\}\, dx = -\int_{x_0-\epsilon}^{x_0+\epsilon} \delta(x - x_0)\, dx, \quad s \geqslant 0, \epsilon > 0,$$

then

$$D\tilde{p}'(x, s)\Big|_{x_0-\epsilon}^{x_0+\epsilon} - v\tilde{p}(x, s)\Big|_{x_0-\epsilon}^{x_0+\epsilon} - \int_{x_0-\epsilon}^{x_0+\epsilon} (s\tilde{p}(x, s))\, dx = -1.$$

In the limit $\epsilon \to 0$, the last two terms at the left-hand side tend to zero due to continuity of $\tilde{p}(x, s)$ at $x = x_0$. While the first summand can be rearranged and evaluated in terms of $\tilde{p}'_<$ and $\tilde{p}'_>$,

$$D(\tilde{p}'_<(x_0) - \tilde{p}'_>(x_0)) = 1,$$

$$\tilde{p}'_<(x_0) = c\frac{\alpha_+ e^{\alpha_+ x_0} - \alpha_- e^{\alpha_- x_0}}{e^{\alpha_+ x_0} - e^{\alpha_- x_0}} = c\frac{\alpha_+ e^{\theta x_0} - \alpha_- e^{-\theta x_0}}{e^{\theta x_0} - e^{-\theta x_0}}. \quad \text{(A3)}$$

Analogously,

$$\tilde{p}'_>(x) = c\frac{\alpha_+^2 e^{\alpha_+(x-1)} - \alpha_-^2 e^{\alpha_-(x-1)}}{\alpha_+ e^{\alpha_+(x_0-1)} - \alpha_- e^{\alpha_-(x_0-1)}}$$

leads to

$$\tilde{p}'_>(x_0) = c\frac{\alpha_+^2 e^{\alpha_+(x_0-1)} - \alpha_-^2 e^{\alpha_-(x_0-1)}}{\alpha_+ e^{\alpha_+(x_0-1)} - \alpha_- e^{\alpha_-(x_0-1)}} = c\frac{\alpha_+^2 e^{\theta(x_0-1)} - \alpha_-^2 e^{-\theta(x_0-1)}}{\alpha_+ e^{\theta(x_0-1)} - \alpha_- e^{-\theta(x_0-1)}}.$$

Therefore, by inserting Eq. (A3),

$$1 = Dc\left(\frac{\alpha_+ e^{\theta x_0} - \alpha_- e^{-\theta x_0}}{e^{\theta x_0} - e^{-\theta x_0}} - \frac{\alpha_+^2 e^{\theta(x_0-1)} - \alpha_-^2 e^{-\theta(x_0-1)}}{\alpha_+ e^{\theta(x_0-1)} - \alpha_- e^{-\theta(x_0-1)}}\right)$$

$$= Dc\,\frac{e^{-\theta}(\alpha_+^2 - \alpha_+\alpha_-) + e^{\theta}(\alpha_-^2 - \alpha_+\alpha_-)}{\alpha_+ e^{\theta(2x_0-1)} + \alpha_- e^{-\theta(2x_0-1)} - \alpha_+ e^{-\theta} - \alpha_- e^{\theta}}$$

$$= 2Dc\,\frac{e^{-\theta}\theta(\theta + \rho) + e^{\theta}\theta(\theta - \rho)}{\alpha_+ e^{\theta(2x_0-1)} + \alpha_- e^{-\theta(2x_0-1)} - \alpha_+ e^{-\theta} - \alpha_- e^{\theta}}$$

$$= 2Dc\,\frac{\theta(\theta\cosh(\theta) - \rho\sinh(\theta))}{\rho\cosh[\theta(2x_0-1)] + \theta\sinh[\theta(2x_0-1)] - \rho\cosh(\theta) + \theta\sinh(\theta)}$$

$$= c\,\frac{\omega(\omega\cosh(\theta) - v\sinh(\theta))}{v\cosh[\theta(2x_0-1)] + \omega\sinh[\theta(2x_0-1)] - v\cosh(\theta) + \omega\sinh(\theta)},$$

which gives

$$c(s) = \tilde{p}(x_0, s) = \frac{v\cosh[\theta(2x_0-1)] + \omega\sinh[\theta(2x_0-1)] - v\cosh(\theta) + \omega\sinh(\theta)}{\omega^2\cosh(\theta) - v\omega\sinh(\theta)}$$

$$= \frac{2\sinh(\theta x_0)\{\omega\cosh[\theta(x_0-1)] + v\sinh[\theta(x_0-1)]\}}{\omega^2\cosh(\theta) - v\,\omega\sinh(\theta)},$$

where ω and θ are defined in Eq. (6). All in all, we obtain Eqs. (8) and (9) for the Laplace transform of the propagator. ■

2. Proof of Proposition III.1

Proof. We first derive $\tilde{f}_0(s)$ using the Laplace-transformed propagator $\tilde{p}(x, s)$ from Lemma II.1. This is done by evaluating the Laplace transform of the probability current $\tilde{J}(x, s)$ from Eq. (3) at the absorbing boundary $x = 0$:

$$\tilde{f}_0(s) = \tilde{J}(0, s) = D\tilde{p}'(0, s) - v\tilde{p}(0, s) = D\tilde{p}'(0, s). \quad \text{(A4)}$$

Simplifying this expression yields Eq. (13) for $s > -v^2/(4D)$, as previously shown in Ref. [77].

We now find a relation between the Laplace-transformed FPT distribution without resetting that we have obtained to the expression with resetting $\tilde{f}_r(s)$. We use a renewal equation that connects the survival function in the resetting case to the survival function for the evolution without resetting. The following equation is well-known in the literature relative to stochastic resetting and can be found, e.g., in Refs. [16–18]:

$$S_r(t) = e^{-rt}S_0(t) + r\int_0^t e^{-ru}S_0(u)S_r(t-u)\,du.$$

By taking the Laplace transform on both sides, we obtain

$$\tilde{S}_r(s) = \tilde{S}_0(s+r) + r\tilde{S}_0(s+r)\tilde{S}_r(s),$$

hence, for all s such that $\tilde{S}_0(s+r) \neq r^{-1}$,

$$\tilde{S}_r(s) = \frac{\tilde{S}_0(s+r)}{1 - r\tilde{S}_0(s+r)}. \quad \text{(A5)}$$

The link between $\tilde{S}_0(s)$ and $\tilde{f}_0(s)$ is provided by the Laplace transform of Eq. (A8), which for $r = 0$ yields, for all $s \neq 0$:

$$\tilde{S}_0(s) = \frac{1 - \tilde{f}_0(s)}{s}.$$

Plugging the latter into Eq. (A5) gives for all $s \neq -r$ such that $\tilde{f}_0(s+r) \neq -s/r$,

$$\tilde{S}_r(s) = \frac{1 - \tilde{f}_0(s+r)}{s + r\tilde{f}_0(s+r)} \quad \text{and} \quad \text{(A6)}$$

$$\tilde{S}_r'(s) = \frac{\tilde{f}_0(s+r) - (r+s)\tilde{f}_0'(s+r) - 1}{\{s + r\tilde{f}_0(s+r)\}^2}. \quad \text{(A7)}$$

Density and survival functions of τ_r are, respectively, given by f_r and $S_r(t) = \int_0^\infty f_r(s)ds$, $\forall t \geqslant 0$, where $r \geqslant 0$. Assuming differentiability, we have

$$f_r(t) = -S_r'(t). \quad \text{(A8)}$$

We obtain from Eq. (A8) the Laplace transform of f_r as $\tilde{f}_r(s) = 1 - s\tilde{S}_r(s)$ for all $s \in \mathbb{R}$. We combine it with Eq. (A6) and it yields the first expression:

$$\forall s > -r,\ \tilde{f}_r(s) = \frac{(s+r)\tilde{f}_0(s+r)}{s + r\tilde{f}_0(s+r)}.$$

This last expression holds $\forall s < -r$ under the assumption $\tilde{f}_0(s+r) \neq -s/r$. We deduce the closed-form expression in Eq. (12) by combining the first expression with $\tilde{f}_0$ in Eq. (13). Note that for the function ω to be defined, we need $s + r \in (-v^2/(4D), \infty)$, viz. $s \in (-r - v^2/(4D), -r)$. ■

3. Proof of Proposition III.2

Proof. The density and survival function of τ_r are, respectively, denoted f_r and $S_r(t) = \int_0^\infty f_r(s)ds$, $\forall t \geqslant 0$, where $r \geqslant 0$. Assuming differentiability, we have Eq. (A8). One shows easily

$$\mathsf{E}\left[\tau_r^p\right] = p\int_0^\infty t^{p-1}S_r(t)\,dt = (-1)^{p-1}p\tilde{S}_r^{(p-1)}(0)$$

for $p = 1, 2\ldots$. In particular,

$$\mathsf{E}[\tau_r] = \tilde{S}_r(0) \ \text{ and } \ \mathsf{E}\left[\tau_r^2\right] = -2\tilde{S}_r'(0). \quad \text{(A9)}$$

Using Eq. (A6) we obtain, for any resetting rate $r > 0$,

$$\mathsf{E}[\tau_r] = \frac{1}{r}\left(\frac{1}{\tilde{f}_0(r)} - 1\right) \quad \text{and} \quad \text{(A10)}$$

$$\mathsf{E}\left[\tau_r^2\right] = -2\frac{\tilde{f}_0(r) - r\tilde{f}_0'(r) - 1}{\{r\tilde{f}_0(r)\}^2} \quad \text{(A11)}$$

$$= \frac{2}{r\tilde{f}_0(r)}\left(\frac{\tilde{f}_0'(r)}{\tilde{f}_0(r)} + \mathsf{E}[\tau_r]\right). \quad \text{(A12)}$$

Thus, Eqs. (A10) and (13) give the desired expectation in Eq. (14).

Here we also provide the most explicit formula:

$$\mathsf{E}[\tau_r] = \frac{1}{r}\left\{\frac{e^{\rho x_0}\left(\omega(r)\cosh\{\theta(r)\} - v\sinh\{\theta(r)\}\right)}{\omega(r)\cosh\{\theta(r)(x_0-1)\} + v\sinh\{\theta(r)(x_0-1)\}} - 1\right\}.$$

For the second moment, we need to differentiate Eq. (13). This leads to

$$\tilde{f}_0'(s) = e^{-\rho x_0}\frac{(v(x_0-1)+2D)\cosh\{\theta(s)(x_0-1)\} + \omega(s)(x_0-1)\sinh\{\theta(s)(x_0-1)\}}{\omega(s)[\omega(s)\cosh\{\theta(s)\} - v\sinh\{\theta(s)\}]}$$
$$+ \tilde{f}_0(s)\frac{(2D-v)\cosh\{\theta(s)\} + \omega(s)\sinh\{\theta(s)\}}{\omega(s)[\omega(s)\cosh\{\theta(s)\} - v\sinh\{\theta(s)\}]}.$$

With this, $\tilde{f}_0'(s)/\tilde{f}_0(s)$ can be simplified to Eq. (15). This with Eq. (A10) give the desired second moment in Eq. (14). ■

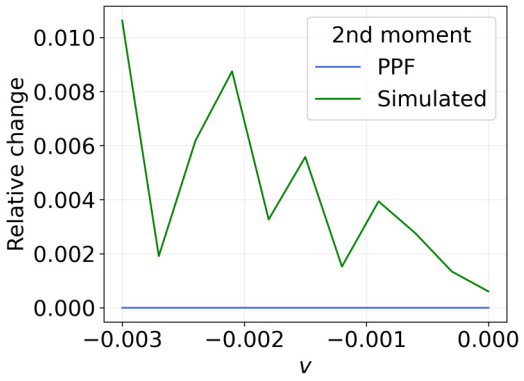

FIG. 7. Relative error of the second moments obtained by PPF and MRA, with respect to the exact second moment and for varying drift parameter v.

4. Proof of Eq. (21) in Remarks III.4

Proof. Before giving the details of the computation of the first two moments of the PPF before the correction in Eq. (19), we first recall that the roots obtained for the partial fraction decomposition α_j must be negative (see Step 3 of Algorithm III.3). So we write $\alpha_j = -|\alpha_j|$, for clarity, and we have

$$\begin{aligned}\mu^{(p)}_{r,m,n} &= \int_0^\infty t^p \sum_{j=0}^{k}\sum_{i=1}^{l_j} \frac{\gamma_{j,i}}{(i-1)!} t^{i-1} e^{-|\alpha_j|t}\, dt \\ &= \sum_{j=0}^{k}\sum_{i=1}^{l_j} \frac{\gamma_{j,i}}{(i-1)!} |\alpha_j|^{-(i+p)} \int_0^\infty t^{i+p-1} e^{-t}\, dt \\ &= \sum_{j=0}^{k}\sum_{i=1}^{l_j} \gamma_{j,i} |\alpha_j|^{-(i+p)} \frac{(i+p-1)!}{(i-1)!}, \quad \text{for } p = 1, 2.\end{aligned}$$

These are the first two moments in Eq. (21). ■

We now provide some numerical complements. Figure 7 below gives the relative error of the second moment by PPF in Eq. (21) and by MRA, with respect to the analytical second moment and for different values of the drift parameter v.

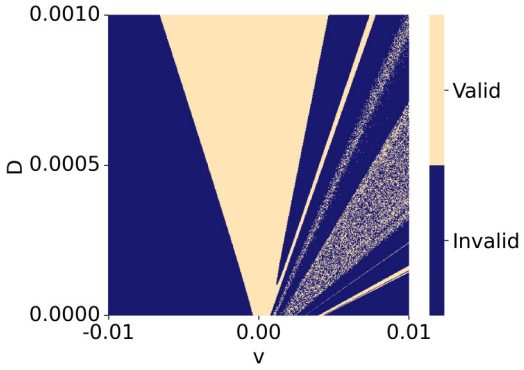

FIG. 8. Parametric space (v, D) of Fig. 4 showing the regions of validity and invalidity of the PPF, with orders $m = 2, n = 3$, $r = (1/3) \times (1/365)$.

Figure 8 is the superposition of the two graphs of Figure 4, thus providing the regions of parametric space (v, D) leading to valid or invalid PPF. The orders are $m = 2, n = 3$, and resetting rate is $r = (1/3) \times (1/365)$.

APPENDIX B: IMPLEMENTATION OF SMRA AND HMRA

1. MRA

We first consider a simple case of the MRA in the time interval [0,1]. In the algorithm, the discretized Wiener process, $\{W_{k,j}\}$, with k, j nonnegative integers, is obtained through Eqs. (24) and (25).

ALGORITHM 1. Basic MRA.

Input: initial position W_0
Output: $\mathbf{W} = \{W_0, \ldots, W_{2^{k-1}}\}, \mathbf{t} = \{0, \ldots, t^\dagger\}$

$k := 0$;
$W_1 := W \sim \mathcal{N}(0,1)$;
$\mathbf{W} := \{W_0, W_1\}$;
$\mathbf{t} := \{0, 1\}$;
while $\mathbf{W}$ *has not reached a stopping condition* **do**
  $k := k + 1$;
  $\mathbf{W}^* := \emptyset$; $\mathbf{t}^* := \emptyset$;
  for $j \in [0, 2^k]$ **do**
    $j' := \lfloor j/2 \rfloor$;
    if j *is even* **then**
      $W_j^* := W_{j'}$; ▷ $W_{j'}$: j'th element of $\mathbf{W}$
      $t_j^* := t_{j'}$; ▷ $t_{j'}$: j'th element of $\mathbf{t}$
    else
      $\mu_{int} := (W_{j'} + W_{j'+1})/2$;
      $\sigma^2_{int} := 2^{-k}$;
      $W_j^* := W \sim \mathcal{N}(\mu_{int}, \sigma^2_{int})$;
      $t_j^* := (t_{j'} + t_{j'+1})/2$;
  $\mathbf{W} := \mathbf{W}^*$;
  $\mathbf{t} := \mathbf{t}^*$;

This pseudocode will generate the two arrays $\mathbf{W}$ and $\mathbf{t}$, the positions and times respectively of the trajectories. The final resolution level k can be arbitrarily obtained with a given stopping condition.

2. Euler-Maruyama trajectory for HMRA

This method is similar to the Euler-Maruyama algorithm described in Algorithm 3, but modified for use in the hybrid algorithm. This code will output two arrays $\mathbf{X}^E$ and $\mathbf{t}^E$ which are Euler-Maruyama trajectories but below a position threshold $\lambda > 0$. This is because above this certain threshold in the position, an absorption is unlikely to happen. Note that reflection and resetting occur in this algorithm.

ALGORITHM 2. euler: Euler traj. below λ.

Input: $X_0, t_0, v, D, r, \Delta t, \lambda$
Output: $\mathbf{X}^E, \mathbf{t}^E$
$X \coloneqq X_0$;
$t \coloneqq t_0$;
$\mathbf{X}^E \coloneqq \emptyset$;
$\mathbf{t}^E \coloneqq \emptyset$;
$t^\dagger \coloneqq t_r \sim \mathrm{Exp}(1/r)$;
while $X > 0$ **do**
  if $t \geq t^\dagger$ **then** ▷ resetting condition
    $X \coloneqq X_0$;
    $t \coloneqq t^\dagger + t_r$, where $t_r \sim \mathrm{Exp}(1/r)$;
  else
    $X \coloneqq X + \Delta X$, where $\Delta X \sim \mathcal{N}(v\,\Delta t, 2D\,\Delta t)$;
    $t \coloneqq \min\{t + \Delta t, t^\dagger\}$;
    if $X \geq 1$ **then** ▷ reflection condition
      $X \coloneqq 2 - X$;
  if $X < \lambda$ **then**
    append X to array $\mathbf{X}^E$;
    append t to array $\mathbf{t}^E$;

3. Euler-Maruyama algorithm

ALGORITHM 3. Euler-Maruyama algorithm for FPT.

Input: $X_0, v, D, r, \Delta t$
Output: τ_r
$X \coloneqq X_0$;
$t \coloneqq 0$;
$t^\dagger \coloneqq t_r \sim \mathrm{Exp}(1/r)$;
while $X > 0$ **do**
  if $t \geq t^\dagger$ **then** ▷ resetting condition
    $X \coloneqq X_0$;
    $t \coloneqq t^\dagger + t_r$, where $t_r \sim \mathrm{Exp}(1/r)$;
  else
    $X \coloneqq X + \Delta X$, where $\Delta X \sim \mathcal{N}(v\,\Delta t, 2D\,\Delta t)$;
    $t \coloneqq \min\{t + \Delta t, t^\dagger\}$;
    if $X \geq 1$ **then** ▷ reflection condition
      $X \coloneqq 2 - X$;
    else if $X \leq 0$ **then** ▷ first passage/stopping condition
      $\tau_r \coloneqq t$;

4. SMRA

This code uses the `multires` function found in Appendix B 1. This algorithm generates a Brownian trajectory $\mathbf{X}_k$, $\mathbf{t}_k$ and outputs its corresponding FPT with the absorbing boundary up to an error threshold ϵ.

Recall the simulation parameters $k^\dagger$ discussed in Sec. IV B. Parameter $k^\dagger$ is the minimum resolution that the trajectory must have before resetting is allowed, while k^* is the maximum resolution before the FPT is recorded and the algorithm is stopped. Note that $k^* > k^\dagger$.

ALGORITHM 4. SMRA.

Input: $x_0, v, D, r, \epsilon, k^*$
Output: τ_r
$t_0 \coloneqq 0$;
$t^\dagger \coloneqq t' \sim \mathrm{Exp}(1/r)$;
$k^\dagger \coloneqq -\left\lceil \dfrac{\log(\epsilon)}{\log(2)} \right\rceil$;
while $\delta_k > \epsilon$ **or** $k < k^*$ **do**
  $k \coloneqq 0$;
  $B_f \coloneqq B' \sim \mathcal{N}(x_0 + v(t^\dagger - t_0), 2D(t^\dagger - t_0))$;
  $\mathbf{B} \coloneqq \{B_0, B_f\}$;
  $\mathbf{t} \coloneqq \{t_0, t^\dagger\}$;
  $\mathbf{X} \coloneqq \{x_0\}$;
  while *all* $X \in \mathbf{X} > 0$ **or** $k < k^\dagger$ **do**
    $k \coloneqq k + 1$;
    $\delta_k \coloneqq \dfrac{t^\dagger}{2^k}$;
    $\mathbf{B}, \mathbf{t} \coloneqq \mathtt{multires}(\mathbf{B}, \mathbf{t}, D, k, t^\dagger)$;
    for $j = 0$ **to** 2^k **do** ▷ reflection condition
      $\Delta B_j \coloneqq B_{j+1} - B_j$;
      $X_{j+1} \coloneqq \min\{X_j + \Delta B_j,\ 2 - (X_j + \Delta B_j)\}$;
    if *any* $X \in \mathbf{X} < 0$ **and** $(\delta_k < \epsilon$ **or** $k > k^*)$ **then** ▷ stopping condition
      $\tau_r = \inf\{t \in \mathbf{t} \mid X_t < 0\}$;
      break loops in lines **3** and **9**
    else if $k > k^\dagger$ **then** ▷ resetting condition
      $t_0 \coloneqq t^\dagger$;
      $t^\dagger \coloneqq t^\dagger + t', t' \sim \mathrm{Exp}(1/r)$;
      break loop in line **9** and **return** to line **3**
    else ▷ increase resolution
      return to line **9**

5. HMRA

This code uses both the `multires` function from Appendix B 1 and the `euler` function from Appendix B 2. The algorithm begins by generating an Euler-Maruyama trajectory $\mathbf{X}^E$ and $\mathbf{t}^E$ below the position threshold λ. Note that the reflections and resets have occurred in the initial Euler-Maruyama trajectory already.

The loop at line 6 splits both $\mathbf{X}^E$ and $\mathbf{t}^E$ into an array of arrays $\mathbf{X}^L$ consisting consecutive elements of the original array, e.g., for $\mathbf{X}^E$: $\mathbf{X}^L = \{\{X_0^E, X_1^E\}, \{X_1^E, X_2^E\}, \ldots\}$. Each array element of both $\mathbf{X}^L$ and $\mathbf{t}^L$ is passed through `multires` and, afterward, the array of arrays is flattened back to a 1D array which is called $\mathbf{X}^M$ and $\mathbf{t}^M$, to check for the first passage and the stopping condition.

ALGORITHM 5. HMRA.

Input: $X_0, v, D, r, \epsilon, \Delta t, k^*, \lambda$
Output: τ_r
$t_0 \coloneqq 0$;
$k \coloneqq 0$;
$\mathbf{X}^E, \mathbf{t}^E \coloneqq \texttt{euler}(X_0, t_0, v, D, r, \Delta t, \lambda)$;
$\mathbf{X}^L \coloneqq \emptyset$;
$\mathbf{t}^L \coloneqq \emptyset$;
for $i = 0$ **to** *length of array* $\mathbf{X}^E$ **do**
  if $(t^E_{i+1} - t^E_i) \leq \Delta t$ **then**
    $X^L_i \coloneqq \{X^E_i, X^E_{i+1}\}$;
    $t^L_i \coloneqq \{t^E_i, t^E_{i+1}\}$;
while $\delta_k < \epsilon$ **do**
  $k \coloneqq k + 1$;
  $\delta_k \coloneqq \dfrac{t^\dagger}{2^k}$;
  for $\ell = 0$ **to** *length of array* $\mathbf{X}^L$ **do**
    $X' \coloneqq X^L_\ell$; ▷ note: $X^L_\ell = \{X^E_i, \ldots, X^E_{i+1}\}_\ell$
    $t' \coloneqq t^L_\ell$; ▷ note: $t^L_\ell = \{t^E_i, \ldots, t^E_{i+1}\}_\ell$
    $X^L_\ell, t^L_\ell \coloneqq \texttt{multires}(X', t', D, k, t^\dagger)$;
  $\mathbf{X}^M \coloneqq$ flattened array of $\mathbf{X}^L$;
  $\mathbf{t}^M \coloneqq$ flattened array of $\mathbf{t}^L$;
  if *any* $X \in \mathbf{X}^M < 0$ **and** $(\delta_k < \epsilon$ **or** $k > k^*)$ **then** ▷ stopping condition
    $\tau_r = \inf\{t \in \mathbf{t}^M \,|\, X^M_t < 0\}$;
    break loop **10**
  else ▷ increase resolution
    return to line **10**

[1] N. G. van Kampen, *Stochastic Processes in Physics and Chemistry*, 3rd ed., North-Holland Personal Library (Elsevier, 2007).
[2] X. Bian, C. Kim, and G. E. Karniadakis, 111 years of Brownian motion, Soft Matter **12**, 6331 (2016).
[3] A. Libchaber, From biology to physics and back: The problem of Brownian movement, Annu. Rev. Condens. Matter Phys. **10**, 275 (2019).
[4] P. Romanczuk, M. Bär, W. Ebeling, B. Lindner, and L. Schimansky-Geier, Active Brownian particles, Eur. Phys. J. Spec. Top. **202**, 1 (2012).
[5] F. Huang and H. Chen, Extremal statistics for a one-dimensional Brownian motion with a reflective boundary, Physica A **633**, 129389 (2024).
[6] P. Romanczuk, I. D. Couzin, and L. Schimansky-Geier, Collective motion due to individual escape and pursuit response, Phys. Rev. Lett. USA **102**, 010602 (2009).
[7] M. L. Woods, C. Carmona-Fontaine, C. P. Barnes, I. D. Couzin, R. Mayor, and K. M. Page, Directional collective cell migration emerges as a property of cell interactions, PLoS ONE **9**, e104969 (2014).
[8] A. Marcovitz and Y. Levy, Obstacles may facilitate and direct DNA search by proteins, Biophys. J. **104**, 2042 (2013).
[9] G. Oshanin, O. Vasilyev, P. L. Krapivsky, and J. Klafter, Survival of an evasive prey, Proc. Natl. Acad. Sci. USA **106**, 13696 (2009).
[10] F. Dufresne and H. U. Gerber, Risk theory for the compound poisson process that is perturbed by diffusion, Insur.: Math. Econ. **10**, 51 (1991).
[11] R. Gatto and B. Baumgartner, Saddlepoint approximations to the probability of ruin in finite time for the compound Poisson risk process perturbed by diffusion, Methodol. Comput. Appl. Prob. **18**, 217 (2016).
[12] R. Gatto and M. Mosimann, Four approaches to compute the probability of ruin in the compound Poisson risk process with diffusion, Math. Comput. Model. **55**, 1169 (2012).
[13] S. N. Majumdar, S. Sabhapandit, and G. Schehr, Dynamical transition in the temporal relaxation of stochastic processes under resetting, Phys. Rev. E **91**, 052131 (2015).
[14] M. R. Evans and S. N. Majumdar, Diffusion with stochastic resetting, Phys. Rev. Lett. **106**, 160601 (2011).
[15] A. Chechkin and I. M. Sokolov, Random search with resetting: A unified renewal approach, Phys. Rev. Lett. **121**, 050601 (2018).

[16] M. R. Evans, S. N. Majumdar, and G. Schehr, Stochastic resetting and applications, J. Phys. A: Math. Theor. **53**, 193001 (2020).

[17] A. Pal and V. V. Prasad, First Passage under stochastic resetting in an interval, Phys. Rev. E **99**, 032123 (2019).

[18] É. Roldán and S. Gupta, Path-integral formalism for stochastic resetting: Exactly solved examples and shortcuts to confinement, Phys. Rev. E **96**, 022130 (2017).

[19] A. Nagar and S. Gupta, Diffusion with stochastic resetting at power-law times, Phys. Rev. E **93**, 060102(R) (2016).

[20] A. Pal, A. Kundu, and M. R. Evans, Diffusion under time-dependent resetting, J. Phys. A: Math. Theor. **49**, 225001 (2016).

[21] L. Kusmierz, S. N. Majumdar, S. Sabhapandit, and G. Schehr, First order transition for the optimal search time of Lévy flights with resetting, Phys. Rev. Lett. **113**, 220602 (2014).

[22] J. M. Meylahn, S. Sabhapandit, and H. Touchette, Large deviations for Markov processes with resetting, Phys. Rev. E **92**, 062148 (2015).

[23] W. Guo, H. Yan, and H. Chen, Extremal statistics for first-passage trajectories of drifted Brownian motion under stochastic resetting, J. Stat. Mech. (2024) 023209.

[24] W. Guo, H. Yan, and H. Chen, Extremal statistics for a resetting Brownian motion before its first-passage time, Phys. Rev. E **108**, 044115 (2023).

[25] G. Mercado-Vásquez and D. Boyer, Lotka–Volterra systems with stochastic resetting, J. Phys. A: Math. Theor. **51**, 405601 (2018).

[26] P. C. Bressloff, Stochastic resetting and the mean-field dynamics of focal adhesions, Phys. Rev. E **102**, 022134 (2020).

[27] É. Roldán and A. Lisica, D. Sánchez-Taltavull, and S. W. Grill, Stochastic resetting in backtrack recovery by RNA polymerases, Phys. Rev. E **93**, 062411 (2016).

[28] A. M. Ramoso, J. A. Magalang, D. Sánchez-Taltavull, J. P. Esguerra, and É. Roldán, Stochastic resetting antiviral therapies prevent drug resistance development, Europhys. Lett. **132**, 50003 (2020).

[29] B. Besga, A. Bovon, A. Petrosyan, S. N. Majumdar, and S. Ciliberto, Optimal mean first-passage time for a Brownian searcher subjected to resetting: Experimental and theoretical results, Phys. Rev. Res. **2**, 032029(R) (2020).

[30] O. Tal-Friedman, A. Pal, A. Sekhon, S. Reuveni, and Y. Roichman, Experimental realization of diffusion with stochastic resetting, J. Phys. Chem. Lett. **11**, 7350 (2020).

[31] G. A. Pavliotis, *Stochastic Processes and Applications: Diffusion Processes, the Fokker-Planck and Langevin Equations*, 1st ed., Texts in Applied Mathematics Vol. 60 (Springer, New York, 2014).

[32] S. Karlin and H. M. Taylor, *A Second Course in Stochastic Processes* (Academic Press, New York, 1981).

[33] S. Redner, *A Guide to First-Passage Processes* (Cambridge University Press, Cambridge, 2001).

[34] S. Iyer-Biswas and A. Zilman, First-passage processes in cellular biology, *Advances in Chemical Physics* (John Wiley & Sons, Ltd., Hoboken, NJ, 2016), Vol. 160, Chap. 5, pp. 261–306.

[35] J. Aguilar, B. A. García, R. Toral, S. Meloni, and J. J. Ramasco, Endemic infectious states below the epidemic threshold and beyond herd immunity, Commun. Phys. **6**, 187 (2023).

[36] Y. Zhang and O. K. Dudko, First-passage processes in the genome, Ann. Rev. Biophys. **45**, 117 (2016).

[37] R. Chicheportiche and J.-P. Bouchaud, Some applications of first-passage ideas to finance, *First-Passage Phenomena and Their Applications* (World Scientific, Singapore, 2014), p. 476.

[38] J. Masoliver and J. Perelló, First-passage and extremes in socio-economic systems, in *First-Passage Phenomena and Their Applications* (World Scientific, Singapore, 2014), pp. 477–501.

[39] M. Maggiore and A. Riotto, The excursion set theory in cosmology, *First-Passage Phenomena and Their Applications* (World Scientific, Singapore, 2014),pp. 532–553.

[40] E. Barkai and D. A. Kessler, *Transport and the First Passage Time Problem with Application to Cold Atoms in Optical Traps, I*: *First-Passage Phenomena and Their Applications* (World Scientific, Singapore, 2014), pp. 502–531.

[41] B. Davies and B. Martin, Numerical inversion of the Laplace transform: A survey and comparison of methods, J. Comput. Phys. **33**, 1 (1979).

[42] S. Asmussen and P. W. Glynn, *Stochastic Simulation: Algorithms and Analysis*, Stochastic Modelling and Applied Probability, Vol. 57 (Springer, New York, 2007).

[43] S. B. Yuste and K. Lindenberg, Comment on "Mean first passage time for anomalous diffusion," Phys. Rev. E **69**, 033101 (2004).

[44] D. L. Dy and J. P. Esguerra, First-Passage characteristics of biased diffusion in a planar wedge, Phys. Rev. E **88**, 012121 (2013).

[45] R. Voituriez and O. Bénichou, First-passage statistics for random walks in bounded domains, *First-Passage Phenomena and Their Applications* (World Scientific, Singapore, 2014), pp. 145–174.

[46] D. R. Cox and H. D. Miller, *The Theory of Stochastic Processes*, 1st ed. (Chapman and Hall/CRC, London, 1965).

[47] A. V. Skorokhod, Stochastic equations for diffusion processes in a bounded region, Theory Prob. Appl. **6**, 264 (1961).

[48] A. Pilipenko, *An Introduction to Stochastic Differential Equations with Reflection*, Lectures in Pure and Applied Mathematics, Vol. 1 (Potsdam University Press, 2014), https://publishup.uni-potsdam.de/opus4-ubp/frontdoor/deliver/index/docId/6949/file/lpam01.pdf.

[49] J. M. Harrison, *Brownian Motion and Stochastic Flow Systems* (John Wiley, New York, 1985).

[50] S. C. Manrubia and E. Lázaro, Viral evolution, Phys. Life Rev. **3**, 65 (2006).

[51] D. Pillay and M. Zambon, Antiviral drug resistance, British Medical J. **317**, 660 (1998).

[52] D. S. Clutter, M. R. Jordan, and S. Bertagnolio, R. W. Shafer, HIV-1 drug resistance and resistance testing, Infect. Genet. Evol. **46**, 292 (2016).

[53] G. A. Whitmore and V. Seshadri, A heuristic derivation of the inverse Gaussian distribution, Am. Stat. **41**, 280 (1987).

[54] R. S. Chhikara and J. Leroy Folks, *The Inverse Gaussian Distribution*, Statistics: A Series of Textbooks and Monographs (CRC Press, Boca Raton, FL, 1988).

[55] Y. L. Luke, On the approximate inversion of some Laplace transforms, Midwest Research Institute, Aerospace Research Laboratories, https://apps.dtic.mil/sti/citations/AD0259669.

[56] I. M. Longman, On the generation of rational function approximations for Laplace transform inversion with an application to viscoelasticity, SIAM J. Appl. Math. **24**, 429 (1973).
[57] J. E. Akin and J. Counts, The application of continued fractions to wave propagation in a semi-infinite elastic cylindrical membrane, J. Appl. Mech. **36**, 420 (1969).
[58] Y. L. Luke, *The Special Functions and Their Approximations*, Mathematics in Science and Engineering Vols. 1 and 2 (Academic Press, New York, London, 1969).
[59] G. A. Baker, Jr. and J. L. Gammel, The Padé approximant, J. Math. Anal. Appl. **2**, 21 (1961).
[60] J. H. Mathews and K. D. Fink, *Numerical Methods Using MATLAB*, 4th ed. (Pearson Prentice Hall, London, San Diego, Cambridge, Oxford, 2004).
[61] R. Gatto, *Stochastische Modelle der Aktuariellen Risikotheorie – Eine Mathematische Einführung*, 2nd ed. (Springer, Berlin, 2020).
[62] A. Talbot, The accurate numerical inversion of Laplace transforms, IMA J. Appl. Math. **23**, 97 (1979).
[63] J. Abate and W. Whitt, A unified framework for numerically inverting Laplace transforms, INFORMS J. Computi. **18**, 408 (2006).
[64] G. F. Lawler, *Introduction to Stochastic Processes*, 1st ed. (Chapman and Hall/CRC, New York, 1995).
[65] R. Gatto, *Stationary Stochastic Models: An Introduction*, 1st ed., World Scientific Series on Probability Theory and Its Applications: Vol. 4 (World Scientific Publishing, Singapore, 2022).
[66] A. Dubey and A. Pal, First-passage functionals for Ornstein-Uhlenbeck process with stochastic resetting, J. Phys. A: Math. Theor. **56**, 435002 (2023).
[67] M. Abundo, The first-passage area of Wiener process with stochastic resetting, Methodol. Comput. Appl. Prob. **25**, 92 (2023).
[68] S. N. Majumdar and H. Orland, Effective Langevin equations for constrained stochastic processes, J. Stat. Mech.: Theory Exp. (2015) P06039.
[69] J. Aguilar, J. W. Baron, T. Galla, and R. Toral, Sampling rare trajectories using stochastic bridges, Phys. Rev. E **105**, 064138 (2022).
[70] J. Aguilar and R. Gatto, Unified perspective on exponential tilt and bridge algorithms for rare trajectories of discrete Markov processes, Phys. Rev. E **109**, 034113 (2024).
[71] J. Aguilar, J. J. Ramasco, and R. Toral, Biased versus unbiased numerical methods for stochastic simulations, Commun. Phys. **7**, 155 (2024).
[72] https://github.com/jarmsmagalang/ppf_approx.
[73] https://github.com/jarmsmagalang/multires.
[74] https://pypi.org/project/ppf-approx.
[75] https://pypi.org/project/multires.
[76] G. B. Arfken, H. J. Weber, and F. E. Harris, *Mathematical Methods for Physicists: A Comprehensive Guide*, 7th ed. (Academic Press, Waltham, Oxford, 2011).
[77] A. Godec and R. Metzler, Universal proximity effect in target search kinetics in the few-encounter limit, Phys. Rev. X **6**, 041037 (2016).